

# Robust semi-parametric signal detection in particle physics with classifiers decorrelated via optimal transport

Purvasha Chakravarti \*

Department of Statistical Science, University College London

Lucas Kania \*

Department of Statistics & Data Science, Carnegie Mellon University

Olaf Behnke

Deutsches Elektronen-Synchrotron (DESY)

Mikael Kuusela and Larry Wasserman

Department of Statistics & Data Science, Carnegie Mellon University

September 11, 2024

## Abstract

Searches of new signals in particle physics are usually done by training a supervised classifier to separate a signal model from the known Standard Model physics (also called the background model). However, even when the signal model is correct, systematic errors in the background model can influence supervised classifiers and might adversely affect the signal detection procedure. To tackle this problem, one approach is to use the (possibly misspecified) classifier only to perform a preliminary signal-enrichment step and then to carry out a bump hunt on the signal-rich sample using only the real experimental data. For this procedure to work, we need a classifier constrained to be decorrelated with one or more protected variables used for the signal detection step. We do this by considering an optimal transport map of the classifier output that makes it independent of the protected variable(s) for the background. We then fit a semi-parametric mixture model to the distribution of the protected variable after making cuts on the transformed classifier to detect the presence of a signal. We compare and contrast this decorrelation method with previous approaches, show that the decorrelation procedure is robust to moderate background misspecification, and analyze the power of the signal detection test as a function of the cut on the classifier.

*Keywords:* Large Hadron Collider, bump hunt, model misspecification, high-energy physics, mixture density fitting, semi-parametric hypothesis testing, algorithmic fairness.

---

\*These two authors contributed equally to this paper. The names are in alphabetical order.

# 1 Introduction

Particle physics aims to understand the structure of matter at a fundamental level, that is, to discern those particles that compose matter but cannot be decomposed. The Standard Model (SM) of particle physics provides the theory behind all known fundamental particles and their interactions. For a long time physicists have theorized the existence of multiple new fundamental particles and are now searching for empirical evidence of the new particles beyond those described by the SM [Evans and Bryant, 2008].

Experiments are conducted at particle colliders to search for these theorized particles. Particle colliders are facilities in underground tunnels where particles are accelerated to almost the speed of light and then made to collide. In the Large Hadron Collider (LHC), the largest collider in the world (27 km long), two protons or heavy ions are accelerated in opposite directions and made to collide within four underground detectors – ALICE, ATLAS, CMS, and LHCb. When a collision occurs, the kinetic energy of the particles transforms into mass, creating new particles [Lyons, 2008]. The new particles formed are often unstable particles, called resonances, which almost instantly decay into other more stable particles. The paths of these particles, along with their momenta and energies, are recorded within the particle detectors. By measuring these, scientists can reconstruct the properties of the unstable particles that gave rise to these more stable, observable particles. Each collision is referred to as an event. Most collisions are considered uninteresting and constitute what physicists call background events. However, some collisions might create the theorized fundamental particles. Hence, the problem is to separate those collisions of interest, called the signal events, from the background events.

Two examples of signal events that we discuss in the experiments of this paper are high-momentum W-boson production and high-mass resonance production. Some theorized new

massive particles are predicted to decay into a final state containing a W boson and other heavy particles [ATLAS, 2018b]. The W boson itself is an unstable resonance and can decay into two quarks, which produce collimated streams of particles, called jets. The presence of the heavy particles causes the W boson to have an unusually high transverse momentum ( $p_T$ ) and the two jets from the W-boson decay to merge into a single large-radius “W-jet”. This is an example of new physics searches where the task is to discriminate the hadronically decaying W bosons (signal events) from the large group of events that produce non-resonant jets (background events). For W boson, the invariant mass of the resulting large-radius jet is a good discriminator from the non-resonant background since the signal is localized in mass, whereas the background is smooth [ATLAS, 2018b]. Finding a mass peak on top of a smooth background has been one of the main techniques in particle physics for discovering new particles. While the W boson itself is a known SM particle, studied in great detail in experiments, the detection of highly boosted W bosons via their mass peak signal can be a strong indirect hint for the presence of new resonances with much higher mass.

However, it is well-established that W-jets have a rich jet substructure. Training boosted decision trees and neural network classifiers on these jet substructure variables (see Table 1 in ATLAS [2018b]) has proven to be particularly successful in increasing the power of detecting the signal events [ATLAS, 2017a,b]. However, these classifiers are trained on Monte Carlo simulations from the hypothesized models, with access to the simulated true labels, but evaluated on unlabelled experimental collision data. Since simulating jets accurately is difficult, there might be systematic differences between the training and the test data. Additionally, the data generation process might not be uniquely specified, with the presence of nuisance parameters, which would also cause differences between the training and test data, affecting the trained classifiers [Louppe et al., 2017].

For the second example, we study production of a high-mass resonance where an exotic high-mass particle decays into two Higgs bosons. The Higgs boson is an unstable particle that decays roughly within  $10^{-22}$  seconds, making it impossible to directly detect it. Instead, the SM predicts that the Higgs boson decays into a pair of bottom quarks (b-quarks) 60% of the time, experimentally shown by ATLAS [2018a] and CMS [2018], which can be used to detect the original resonance. To detect this, one needs to investigate the events where four b-quarks are observed and detect in which events the four b-quarks originate from the resonance (signal events) versus events where the four b-quarks were produced by a different process (background events). The background process is dominated by jet production via strong interactions of quarks and gluons from the colliding protons. The b-quarks themselves hadronize to form streams of other particles and their final stable decay products can be reconstructed in the detectors as so-called b-jets. The kinematic properties of the four b-jets (e.g., momentum, energy, angles, etc.) can then be used to detect if a particular event is likely to be a high-mass resonance event. Similar to W-boson production, the invariant mass can also be used to identify signal events from background events.

The distribution of the signal in this case can be approximated accurately, however, simulating the background distribution in this case suffers from being computationally intractable due to the presence of large higher-order perturbative corrections in strong interactions [Di Micco et al., 2020]. Previous research has assumed that there are auxiliary events that are related to the background distribution via a distributional shift and can be used to estimate the background distribution [Bryant, 2018, Manole et al., 2022]. An example of such auxiliary events would be events that result in less than four b-quarks, making them impossible to have come from a signal event, but having similar kinematic

properties as the background [Bryant, 2018]. Since the background distribution is now being estimated, the background samples might not be entirely accurate, and hence, similar to W-boson production, a signal detection test based on a classifier trained on these samples might be affected.

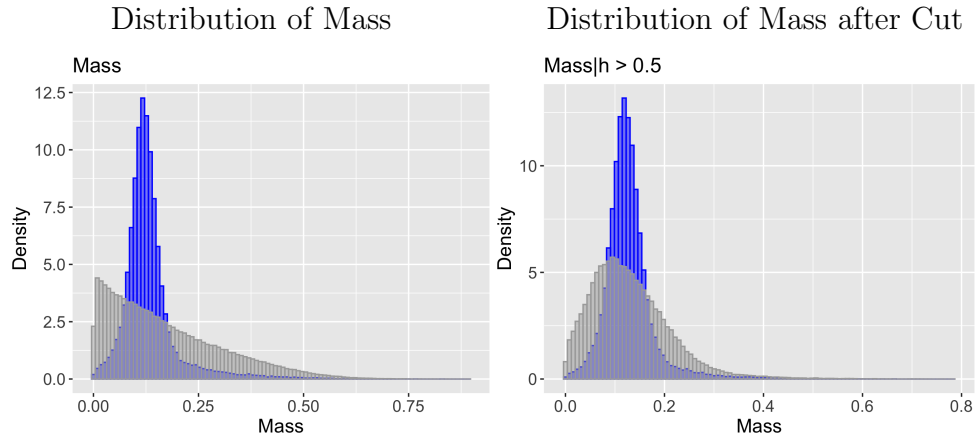


Figure 1: Evidence of sculpting in the shape of the background distribution of the invariant mass (protected variable) after a classifier-based filtration, where a cut is performed on the jet substructure (auxiliary variables) classifier output ( $h$ ) at  $h > 0.5$ . The grey bars represent the background, and the blue bars represent the signal. Cutting on the classifier output sculpts the background distribution of the protected mass variable, creating an artificial bump that could be confused with the signal mass peak.

The solution in these cases is to use a variable in which the signal detection test can be performed without having access to reliable background samples. A common choice is a variable in which the signal is localized and the background is smooth, so that the signal detection test can be performed as a bump hunt [CDF Collaboration, 2009, Choudalakis, 2011]. In the above examples, the invariant mass is such a variable. However, given the additional information available in the form of supervised classifiers trained on auxiliary

variables (e.g., jet substructure variables for W boson and kinematic variables for the high-mass resonance event), we would ideally like to use these to perform a filtering step to enhance the signal before using the invariant mass for the actual test. The output of these classifiers exhibits non-linear dependence with the invariant mass, and therefore, a filtration based on the classifiers causes a distortion to the shape of the invariant mass distribution for the background events, making it hard to distinguish it from the signal events. This phenomenon is called *sculpting* [ATLAS, 2018b] and is shown in Figure 1. This will be discussed in more detail in Section 1.2. The objective is to find a classifier given the constraint that it is decorrelated (in fact, what we want is independence, but decorrelation has become the standard term in high-energy physics) with invariant mass [ATLAS, 2018b]. More generally, we want to produce a classifier that is decorrelated with respect to one or more *protected variables* in which the bump hunt will be performed.

The main objective of this paper is, thus, to present a data analysis pipeline consisting of a decorrelation algorithm and a signal detection test and show the robustness of the framework to systematic mis-modeling of the background data. We also show through our experiments that using the decorrelated classifiers to incorporate auxiliary information does indeed increase the power of the signal detection test, while filtering using correlated classifiers yields unreliable tests due to sculpting. In the rest of the introduction, we introduce in greater detail the signal detection test using the invariant mass, the idea of decorrelation, and our contributions.

## 1.1 Introduction to bump hunting

The detection of new physical phenomena in high-energy physics has historically relied on the search for resonances causing a bump in the invariant-mass spectrum of their daughter

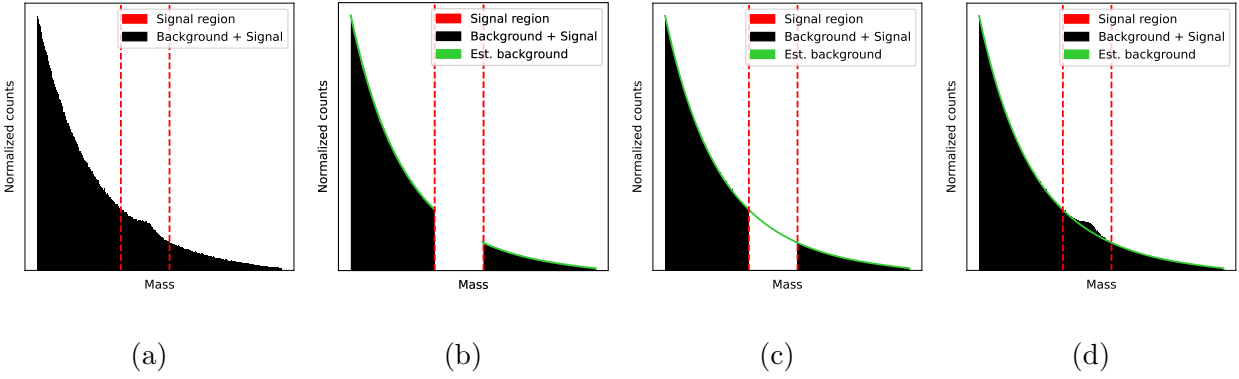


Figure 2: Pictorial representation of bump hunting. (a) Unlabeled mixture data of background and signal events. (b) Background estimation from control region. (c) Background interpolation into signal region. (d) Signal detection.

particles. The shape of the bump is driven by the natural width of the resonance as well as by detector resolution effects. Physical background processes are known to usually produce smooth mass distributions. Thus, the presence of deviations from this pattern can provide evidence for the existence of undiscovered phenomena. Although physicists might not know the exact background or signal distributions, they can often pinpoint regions of the invariant mass spectrum where they expect to observe a resonance if it exists. These are called signal regions. These two assumptions, smoothly decaying background and known signal regions, can be used to perform signal detection. To make the ideas concrete, consider figure 2a, which presents an idealized scenario in which we have data from a mixture of background and signal events and a predefined signal region. First, the background is estimated while censoring the signal region; see Figure 2b. Second, the fitted background is interpolated to the signal region; see Figure 2c. Finally, the interpolated fitted background and observed distribution in the signal region are compared to check if they differ significantly; see Figure 2d. Informally, physicists look for bumps on the interpolated background.

This methodology is called *bump hunting* [CDF Collaboration, 2009] and goes back at

least to the discovery of the  $\rho$  meson [Button et al., 1962]. A successful improvement has been the **BumpHunter** algorithm [Choudalakis, 2011] that searches the entire invariant mass spectrum using a moving signal region while accounting for performing multiple hypothesis tests, called the *look elsewhere effect* in the physics literature [Gross and Vitells, 2010]. The algorithm has been widely used together with parametric and non-parametric background estimation [ATLAS Collaboration, 2010, CDF Collaboration, 2009]. Modern developments have focused on using machine learning both to estimate the background and to improve the sensitivity of signal tests through classifiers [Kasieczka et al., 2021]. For instance, Collins et al. [2019] uses classifiers to enrich the signal region, and then proceeds to perform a likelihood ratio test with a parametric background and model-free signal using the asymptotic formulae proposed by Cowan et al. [2011]. Although asymptotically valid, such an approach is not necessarily optimal. In this work, we prove the asymptotic optimality of the proposed via the semi-parametric framework. That is, the proposed test asymptotically makes the most efficient use of the available data while allowing for an arbitrarily complex signal contained in the signal region.

## 1.2 Introduction to decorrelation

Bump hunting requires a reasonably large signal strength in order to detect the presence of signal events. However, in many scenarios for new physics searches, the expected signal strengths are small compared to the SM background, leading to negligible power when testing. As mentioned before, an approach taken by physicists is to use available auxiliary variables to train a supervised classifier ( $h$ ) on assumed background and signal samples, and use the classifier to identify signal-rich regions where the background is most suppressed. The bump hunt search is then performed on the data within this signal-rich region [AT-



LAS, 2018b]. To find the signal-rich region, one just performs pre-determined *cuts* on the classifier output, e.g., if the cut-off is  $t$  and the classifier is trained so that large values correspond to signal events, the signal-rich region is given by  $\{x : h(x) > t\}$ . Note that this is different from the signal region mentioned above and illustrated in Figure 2a, since the signal-rich region is in the domain of the auxiliary variables whereas the signal region is in the domain of the protected variable(s).

The problem is that since the detection is now performed conditional on the classifier output, the distribution of the protected variable on which the signal detection is performed, changes (sculpts). As shown in Figure 1, the distribution of the protected variable (mass) for the background data (grey) before signal enrichment is a smoothly falling curve, whereas after signal enrichment, the distribution of the background itself has a bump, making it hard to distinguish it from the signal. This would make the bump-hunt test lose validity since under the null case itself, the data has a bump.

So, we need to ensure that the distribution of the protected variable remains unchanged for the background data after signal enrichment. This can be easily guaranteed if the classifier output is independent of the protected variable. This can be achieved in three ways: (1) Make the input variables of the classifier independent of the protected variable. (2) Enforce the classifier to be independent of the protected variable during training. (3) Transform any pre-trained classifier to be independent of the protected variable by composing the classifier output with an additional mapping. Our algorithm CDOT (Classifier Decorrelated using Optimal Transport) takes this approach using an optimal transport map.

For the first approach, early works solved the problem by using theoretical domain knowledge to modify the auxiliary variables to be independent of the protected variable before training the classifier. Designing Decorrelated Taggers (DDT) [Dolen et al., 2016],

uses a simple parametric function to modify the auxiliary variable to avoid sculpting. The Convolved SubStructure (CSS) approach [Moult et al., 2018] finds analytically a convolution such that when it is applied on the auxiliary variables, they theoretically become independent of the protected variable. Note that both of these methods are specific to particular experiments (W-boson production) and do not utilize the full potential of all available auxiliary variables.

A standard way to perform decorrelation during the training stage is to add a penalty term to the classification loss function when fitting the classifier. Multiple penalty terms have been considered in past literature, e.g., DisCo [Kasieczka and Shih, 2020] uses the distance correlation. Adversarial Neural Networks (ANN) [Shimmin et al., 2017, Louppe et al., 2017] use as penalty the accuracy of a second adversary neural network that predicts the protected variable from the classifier output, maximizing classification accuracy while minimizing the dependence of the classifier output on the protected variable. Moment Decomposition (MoDe) [Kitouni et al., 2021], on the other hand, argues that we do not need independence, instead they ensure that the trained penalized classifier does not introduce a localization (bump) in the background by adding a penalty based on the moments of the protected variable’s CDF. Outlier exposure variational autoencoders (OE-VAE) [Cheng et al., 2023] use a variational autoencoder in place of a classifier to find a latent space where they perform anomaly detection to tag anomalous jets. The penalty they use is the loss of a second classifier that separates out-of-distribution events from in-distribution events where the out-of-distribution events are resampled such that the protected variable’s distribution is the same as that of the in-distribution events.

For the last approach, both our approach and the one taken in a parallel body of work CNOTS [Algren et al., 2024] is to find a transformation of a pre-trained classifier that

makes it independent of the protected variable using an optimal transport map [Villani, 2021]. However, the methods diverge in the way they estimate this optimal transport map. While in our work we find a closed-form solution to the optimal transport problem and estimate it using conditional kernel density estimators, CNOTS uses the Kantorovich dual formulation of the optimal transport problem to show that the optimal transport map can be written as the gradient of a convex neural network, resulting in a map that is monotonic. The authors then fit two partially input convex neural networks (PICNNs) to estimate this. CNOTS [Algren et al., 2024] additionally handles multivariate classifiers whereas we address univariate classifiers. We however note that while our method can be extended to the multivariate classifier case, the optimal transport problem does not have a closed-form solution in that case (except for when they are normally distributed), which would make it computationally expensive.

A previous work, Klein and Golling [2022], uses a conditional normalizing flow that finds a map between the distribution of the classifier conditioned on the protected variables and a known distribution using a neural network and uses this to transform the classifier to a decorrelated classifier. Another similar method [Moreno et al., 2020] takes a slightly different approach. Instead of transforming the classifier, they change the cut threshold such that the distribution of the protected variable after the cut remains unchanged for the background. They perform quantile regression of the classifier output on the protected variable to estimate the threshold as a function of the protected variable corresponding to a particular quantile  $t$ . In theory, this is identical to finding a transformed classifier and fixing the threshold at  $t$ , but the way the estimation is performed in practice is different. Additionally, in this case the threshold is a random variable that varies with the protected variable.

### 1.3 Contributions

In this paper, our main contribution is to present a complete pipeline for signal detection using a decorrelated classifier and provide a statistical analysis of the entire pipeline. We study—to the best of our knowledge, for the first time—how implementing a classifier filtration and a decorrelation algorithm before performing a bump hunt affects the power and validity of the signal detection test compared to not implementing them. The pipeline consists of the following steps:

1. Training Classifier: Train a classifier to separate signal from the background using auxiliary variables.
2. Signal Enrichment: (a) Apply the proposed decorrelation algorithm based on optimal transport to the trained classifier. (b) Filter data using the decorrelated classifier.
3. Signal Detection: Use a semi-parametric bump-hunt test on the filtered data to perform signal detection.

The entire proposed pipeline is demonstrated in Figure 3.

The decorrelation algorithm we propose and discuss in this paper though similar to Algren et al. [2024] (as mentioned above), differs in the way we estimate the optimal transport map. Both methods are applicable to multivariate protected variables. The Algren et al. [2024] method is additionally applicable to multivariate classifiers as well. We additionally show that the proposed decorrelation algorithm can be extended via geodesic morphing to give rise to a range of decorrelated classifiers with varying degrees of decorrelation. The intermediate stages provide higher signal vs. background separation than the completely decorrelated classifier and higher decorrelation than the original classifier. We further compare our proposed decorrelation method with previous decorrelation methods as a function

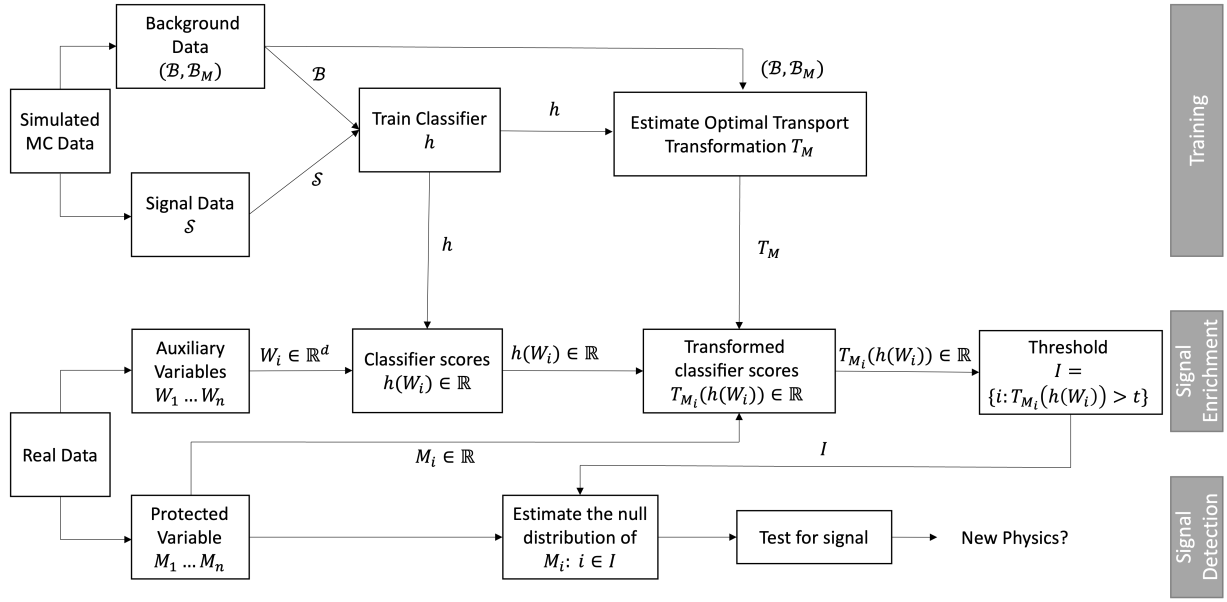


Figure 3: Flowchart of the signal detection process. The process can be divided into three stages - training, signal enrichment, and signal detection stages. In the training stage, we use the Monte Carlo (MC) simulated background and signal data to train the supervised classifier  $h$  as well as the optimal transport map  $T_M$  to get the classifier decorrelated through optimal transport (CDOT),  $T_M(h(\cdot))$ . In the signal enrichment stage, we threshold the trained CDOT on the real experimental data. Finally, in the signal detection stage we use the protected variable for the selected real data to perform bump-hunt signal detection.

of the degree of decorrelation and demonstrate the superiority of the method for high levels of decorrelation.

Regarding bump hunting [CDF Collaboration, 2009, Choudalakis, 2011], for flexible parametric background distributions and arbitrary signal distributions, we propose a test based on the protected variable and prove its optimality in the semi-parametric framework [van der Vaart, 1998]. Informally, the optimality guarantees that the proposed test makes the best of use of the available information when the signal can be arbitrarily complex but contained in the signal region. The test is based on computing the maximum likelihood

estimator while censoring the signal region, and can be connected to previous work on counting experiments and interpolating the background distribution on the signal region [Behnke et al., 2013]. Since the test is performed after the signal enrichment step, we propose a simple model selection procedure based on sample splitting to empirically calibrate the test under the null distribution.

Finally, we perform a thorough study of the robustness of the signal detection pipeline to systematic mismodeling in the background. To the best of our knowledge, such robustness study has not appeared in previous decorrelation literature. Furthermore, we study the power and validity of the signal detection test with and without decorrelation and with and without signal enrichment, and conclude that decorrelation and signal enrichment help produce a stable, robust, valid and more powerful test. Lastly, one of our objectives is to introduce the idea of decorrelation to statisticians since it has potential applications in algorithmic fairness.

## 2 Methods

As discussed in the introduction in Section 1, we have three sources of data at hand

$$\text{MC Background } (\mathcal{B}) : X_1, \dots, X_{m_b} \sim p_b$$

$$\text{MC Signal } (\mathcal{S}) : Y_1, \dots, Y_{m_s} \sim p_s$$

$$\text{Experimental/Real data } (\mathcal{E}) : W_1, \dots, W_n \sim q = (1 - \lambda) \cdot p_b + \lambda \cdot p_s$$

Here  $p_b$ ,  $p_s$  and  $q$  are the densities of the simulated background, the simulated signal and the experimental data, respectively.  $\lambda \in [0, 1]$  is the signal strength which represents the probability of a signal event in the experimental data. Furthermore, we have data on the protected variable  $M$ , for all the three samples, i.e.,  $M_{X_i} \sim p_{bM}$ ,  $M_{Y_i} \sim p_{sM}$  and

$M_{W_i} \sim q_M$ . Henceforth, we will drop the  $M$  from the density notation to interchangeably use  $p_b$ ,  $p_s$  and  $q$  for the protected variable as well, since from context it should be clear which density we mean. We want to perform a signal detection test, i.e., test  $H_0 : \lambda = 0$ . As discussed in Section 1, since the signal is localized in the protected variable  $M$ , the test is performed on the protected experimental data  $M_{W_i} \sim q = (1 - \lambda)p_b + \lambda p_s$ . Additionally, as explained in the introduction, we do not entirely trust the background simulations. So, it is important to note that we do not use the background or signal simulations for the actual test. Hence, the test is able to robustly detect any signal that is localized in the protected variable, even if the background simulation is mis-specified.

Let  $S \in \{0, 1\}$  be an indicator for a signal event. Now, let  $Z = h(W) = \hat{\mathbb{P}}(S = 1|W)$  denote the output of a probabilistic classifier that separates background and signal data. The joint density of  $(Z, M)$  can be written as:

$$\begin{aligned} p(z, m) &= p(z)p(m|z) \\ &= p(z)[p(m|z, S = 0)\mathbb{P}(S = 0|z) + p(m|z, S = 1)\mathbb{P}(S = 1|z)] \\ &= p(z)[(1 - \lambda(z))p(m|z, S = 0) + \lambda(z)p(m|z, S = 1)], \end{aligned}$$

where  $\lambda(z) = \mathbb{P}(S = 1|Z = z)$ . Now,  $\lambda = \mathbb{P}(S = 1) = \int \lambda(z)dP(z)$ . We want to perform a signal detection test, i.e., test  $H_0 : \lambda = 0$ . But as described in Section 1, we want to perform the test after performing signal enrichment. So, we perform the test on experimental data that passes the cut:  $h(W) > t$ , where  $t > 0$  is some fixed threshold. That is, instead of  $\lambda$  we are now interested in  $\lambda(z)$  for  $z > t$ . Note that under the null,  $H_0 : \lambda = 0$ , we also have  $\lambda(z) = 0$  for all  $z$ . Also, note that we expect  $\lambda(z)$  to increase as  $z$  increases since the classifier is trained to detect signal, so higher classifier output indicates a higher chance of the event being a signal event.

The selected data are now conditional on  $Z = h(W) > t$ . Considering the density

$p(z, m|Z > t)$ , this has two effects: we are now interested in  $\lambda(z)$  for  $z > t$  which is larger than  $\lambda$ , so it increases the signal strength in the test data (good) but it replaces  $p_b(m)$  and  $p_s(m)$  with  $p_b(m|Z > t)$  and  $p_s(m|Z > t)$  which are closer together (bad) causing sculpting. Ideally, we want the optimal classifier subject to the condition:  $p_b(m|z) = p_b(m)$  and  $p_s(m|z) = p_s(m)$ . It is impossible to satisfy both of these conditions at once but in practice, it is sufficient to have  $Z = h(W)$  such that  $p_b(m|z) = p_b(m)$ , i.e.,  $h$  is constructed so that  $h(X)$  is independent of  $m(X)$ , given that  $X$  is from the background distribution  $p_b$ . It is also important to note that as the amount of enrichment increases, i.e.,  $t$  increases, while  $\lambda(z)$  increases, the sample size decreases and hence too much enrichment could potentially reduce power. So there is a trade-off between sample size and increasing  $\lambda(z)$  and one needs to be careful when choosing  $t$ . So, now the joint density of  $(Z, M)$  becomes:

$$\begin{aligned}
p(z, m) &= p(z)[(1 - \lambda(z))p(m|z, S = 0) + \lambda(z)p(m|z, S = 1)] \\
&= p(z)[(1 - \lambda(z))p_b(m|z) + \lambda(z)p_s(m|z)] \\
&= p(z)[(1 - \lambda(z))p_b(m) + \lambda(z)p_s(m|z)] \quad \text{due to decorrelation.}
\end{aligned}$$

As mentioned in the introduction, the proposed signal detection workflow has three steps:

- (Step 1): Training and Decorrelation: Train a probabilistic classifier ( $h$ ) on the simulated signal and simulated background data to identify signal events. Then apply a transformation ( $T_M(h)$ ) to decorrelate it, i.e., make it independent of the protected variable ( $M$ ) for the background. We present the decorrelation procedure where we find the transformation  $T_M$  using optimal transport in more detail in Section 2.1.
- (Step 2): Signal Enrichment: Filter the experimental data ( $W$ 's) using the classifier selecting a signal-rich sub-sample  $E_t = \{i : T_{M_i}(h(W_i)) > t\}$  for some threshold  $0 < t < 1$ .



(Step 3): Signal Detection: We perform a bump-hunt on the protected variable for the selected experimental data, i.e., on  $M_{W_i}$  for  $i \in E_t$ . Let  $M$  be distributed as:

$$q(m) = (1 - \lambda) \cdot p_b(m) + \lambda \cdot p_s(m) \quad (1)$$

Here,  $p_b(m)$  is a smooth background model, and  $p_s(m)$  is a bump-like function.

We additionally have for the selected experimental data:

$$q(m|Z > t) = (1 - \lambda_t) \cdot p_b(m) + \lambda_t \cdot p_s(m|Z > t) \quad (2)$$

where  $Z = T_M(h(W))$  is the new transformed classifier and  $\lambda_t = \mathbb{P}(S = 1|Z > t)$ .

We fit  $q(m|Z > t)$  using the selected experimental data,  $M_{W_i}$  for  $i \in E_t$ , and test  $H_0 : \lambda_t = 0$  versus  $H_1 : \lambda_t > 0$ . We discuss the signal detection in detail in Section 2.2.

For the implementation of Step 1, we split the simulated background data into a training data set and a validation data set, where the training data set is used to train the probabilistic classifier and the validation data set is used to train the decorrelation algorithm. We train a random forest classifier as the probabilistic classifier  $h$  that separates the signal from the background. But, one could use any pre-trained probabilistic classifier and then decorrelate it for the background using the decorrelation algorithm presented in this paper.

## 2.1 Decorrelation via Optimal Transport

As mentioned above, the goal of the decorrelation procedure is to construct  $h$  so that  $h(X)$  is independent of  $m(X)$ , given that  $X$  is from the background distribution  $p_b$ . In this section, we discuss a few options of the ways in which this decorrelation can be done and discuss our proposed algorithm in detail.

One option is to transform the data  $X$  itself to make it independent of  $M$  subject to making the transformed data as close to the original data as possible while keeping the marginal distribution of  $X$  intact. If  $X$  itself is independent of  $M$ , then any classifier applied to it is also independent of  $M$ , and hence any classifier can be used. However, if  $X$  is high-dimensional, this is computationally expensive due to the lack of a closed-form expression for optimal transport maps in high-dimensions.

As a more practical alternative, we consider transforming the classifier  $h(X)$  to be independent of  $M$  for the background data  $X \sim p_b$ , such that the transformed classifier output is as close to the original as possible, while keeping the marginal distribution the same. Note, without loss of generality, one could choose any distribution for the new marginal distribution. We decided to keep the marginal distribution unchanged. One way to achieve this transformation is by solving the optimal transport problem given by: minimize  $\mathbb{E}[(T_M(Z) - Z)^2]$  subject to  $T_M(Z)$  independent of  $M$  and  $p_{bT_M(Z)}(z) = p_b(z)$ , where  $Z = h(X)$  and  $p_{bT_M(Z)}$  and  $p_b$  are the marginal densities of  $T_M(Z)$  and  $Z$ , respectively. The solution to this optimization problem is given by the optimal transport map  $T_m$  from  $p_b(z|m)$  to the marginal  $p_b(z)$ . This is shown in Lemma 3 in Appendix A. Additionally, as our classifier  $Z = h(X)$  is univariate,  $T_m$  has a closed-form solution given by  $T_m(z) = F_z^{-1}(F_{z|m}(z))$  where  $F_z$  is the marginal cdf of  $Z = h(X)$  and  $F_{z|m}$  is the conditional cdf of  $Z$  given  $M = m$  for  $X \sim p_b$ .

So, to estimate the optimal transport map  $T_m$ , we first need to estimate  $F_z$ , the marginal cdf of  $Z$  and  $F_{z|m}$ , the conditional cdf of  $Z$  given  $M = m$ , where  $Z = h(X)$  is the classifier output on the background data  $X$ . To estimate  $F_z$ , we use the empirical cdf of the background data  $h(X_i)$  to obtain an estimate  $\widehat{F}_z(t)$ . Since we have sufficient background data, this is a good estimate of the marginal cdf.

Estimating the conditional cdf  $F_{z|m}$  poses a more challenging task. We use a kernel conditional distribution estimator (using `npcdist` in R package `np` [Li and Racine, 2008, Hayfield and Racine, 2008, Li et al., 2013]) to estimate the conditional cdf. The challenge is that we need to find two optimal bandwidths for the kernel estimator, one along the  $z$  dimension and one along the  $m$  dimension. We note in our experiments that a fixed bandwidth works along the  $z$  dimension, however, the optimal bandwidth along the  $m$  dimension varies with the protected variable  $M$ . Finding an adaptive optimal bandwidth with  $M$  is computationally expensive, so instead we take one of two approaches. The first simpler approach is to assume that the optimal bandwidth along  $M$  changes as a step function of  $M$ , where the points at which it changes are visibly observable from the distribution of  $M$  and the optimal bandwidth along  $Z$  remains constant. The second approach is to assume that a particular location-scale transformation of  $Z$  as a function of  $\log(M)$  results in a constant optimal bandwidth for the kernel estimator of  $F_{z|m}$ . Specifically, we assume

$$\text{logit}(Z) = \mu(M) + \sigma(M)\epsilon,$$

where  $\mu(M) = E[\text{logit}(Z)|\log(M)]$ ,  $\sigma^2(M) = \text{Var}(\text{logit}(Z)|\log(M))$ , and the conditional distribution estimator of  $\epsilon|\log(M)$  has a fixed optimal bandwidth. The intuition behind taking the *logit* and *log* transformations comes from the context of  $Z = h(X)$  being a classifier output and the protected variable  $M$  usually being the invariant mass, which is a positively-skewed variable. Depending on the data set, the *logit* and *log* transformations may or may not be necessary.

Using this assumption, we estimate  $\hat{\eta}_i = \text{logit}(h(X_i)) - \hat{\mu}(M_{X_i})$ , where  $\hat{\mu}$  is an estimator of  $\mu$  derived using non-parametric regression of  $\text{logit}(h(X))$  on  $\log(M)$ . Then we can estimate  $\hat{\sigma}^2(M_{X_i})$ 's using a non-parametric regression of  $\hat{\eta}^2$  on  $\log(M)$ . Now, we can estimate  $\epsilon$  using  $\hat{\epsilon}_i = \hat{\eta}_i/\hat{\sigma}(M_{X_i})$  and estimate  $F_{\epsilon|m}$  using a fixed-bandwidth conditional distribution

estimator  $\widehat{F}_{\epsilon|m}$ . Then the conditional distribution of  $Z|M$  can be derived as

$$\begin{aligned}
F_{z|m}(t) &= P(Z \leq t | M = m) \\
&= P(\text{logit}(Z) \leq \text{logit}(t) | M = m) \\
&= P(\mu(M) + \sigma(M)\epsilon \leq \text{logit}(t) | M = m) \\
&= P\left(\epsilon \leq \frac{\text{logit}(t) - \mu(M)}{\sigma(M)} \middle| M = m\right) = F_{\epsilon|m}\left(\frac{\text{logit}(t) - \mu(M)}{\sigma(M)}\right).
\end{aligned}$$

Therefore,

$$\widehat{F}_{z|m}(t) = \widehat{F}_{\epsilon|m}\left(\frac{\text{logit}(t) - \widehat{\mu}(M)}{\widehat{\sigma}(M)}\right). \quad (3)$$

The CDOT (Classifier Decorrelated via Optimal Transport) procedure is detailed in Algorithm 1 in Appendix A.

**Remarks:**

1. It is important to note that even though we call the classifier a decorrelated classifier in accordance with standard terminology in HEP, in reality the transformed classifier  $T_M(h)$  is independent of  $M$  for the background data and not just uncorrelated.
2. The best approach to estimate the conditional distribution of  $Z|M$  (specifically the optimal bandwidth along the  $m$ -axis) in Step 3 of Algorithm 1 in Appendix A, depends on the distribution of  $M$  and  $Z|M$  for the background data. We can use the available background validation data to decide which approach is better for a particular dataset.

The optimal transport map  $T_m(h)$  transports  $p_b(z|m)$  to the marginal  $p_b(z)$  for every fixed  $m$ . An additional contribution of this paper is to consider the optimal path or geodesic taken by the optimal transport map, i.e, to look at the intermediate steps of the transport problem. Let  $\mathcal{F}$  be the set of all distributions and  $g_m : [0, 1] \rightarrow \mathcal{F}$  is such that  $g_m(0) = p_b(\cdot|m)$  and  $g_m(1) = p_b(\cdot)$ . Then  $\{g_m(t) : 0 \leq t \leq 1\}$  is a path connecting

$p_b(z|m)$  and  $p_b(z)$ . The geodesic is the shortest path connecting  $p_b(z|m)$  and  $p_b(z)$  and it can be shown that for the geodesic path  $\{g_m(t) : 0 \leq t \leq 1\}$ , the transformation corresponding to an intermediate point in the path  $g_m(t)$  is given by  $th + (1-t)T_m(h)$ , i.e.,  $p_b(th + (1-t)T_m(h)|m) = g_m(t)$  [Villani, 2021]. Hence, the geodesic gives rise to a range of decorrelated classifiers with varying degrees of decorrelation.

## 2.2 Semi-parametric efficient test for signal detection

We propose an efficient test for the presence of a signal using only the protected variable  $M$ , which is usually the invariant mass. We assume that the support of its distribution, denoted by  $\Omega$ , can be split into disjoint control and signal regions, denoted by  $\mathbb{C}$  and  $\mathbb{S}$  correspondingly. Furthermore, we assume that the signal region is known. In the following, we rewrite the conditional mixture after the signal enrichment step, see eq. (2), streamlining the notation in order to simplify the presentation of this section. The model is:

$$M_1, \dots, M_n \stackrel{\text{iid}}{\sim} f(m) = (1 - \lambda) \cdot b(m) + \lambda \cdot s(m) \quad (4)$$

$$\text{s.t. support}(f) = \Omega = \mathbb{S} \cup \mathbb{C} \text{ , } \mathbb{S} \cap \mathbb{C} = \emptyset \text{ and } \int_{\mathbb{S}} s(m) dm = 1 \quad (5)$$

where  $f(m) = q(m|Z > t)$  is the mixture density,  $b(m) = p_b(m)$  is the background density,  $s(m) = p_s(m|Z > t)$  is the signal density and  $\lambda = \lambda_t = P(S = 1|Z > t)$  is the signal strength. Note that we have suppressed the dependence on the threshold  $t$  in all cases. The above is a semi-parametric model [van der Vaart, 1998, Kosorok, 2008] because the signal distribution is (except that it is supported on the signal region) but the background is assumed to either be known or parametric. Formally, given the above  $n$  observations from the previous mixture eq. (4), we propose a test that decides between the null hypothesis, ie no signal present  $H_0 : \lambda = 0$ , and the alternative hypothesis  $H_1 : \lambda > 0$ . Recall that a test is a function of the data  $\Psi_\alpha : \text{support}(f) \rightarrow \{0, 1\}$  that returns 0 if it considers that

the data support the null hypothesis and 1 otherwise. We say that a test is asymptotically valid if it asymptotically controls the type I error, that is,  $\lim_{n \rightarrow \infty} P(\Psi_\alpha(F_n, B) = 1) \leq \alpha$ .

Throughout this section, we adopt the following conventions: if  $b$  denotes a density, then  $B(A)$  indicates its integral over the set  $A$ , i.e.  $B(A) = \int_A b$ . Analogously, let  $F_n(m) = F_n((-\infty, m]) = n^{-1} \sum_{i=1}^n I(M_i \leq m)$  denote the empirical CDF and  $F_n(A) = n^{-1} \sum_{i=1}^n I(M_i \in A)$  its integral over the set  $A$ .

To gain some insight, consider the case where the background is known. It can be immediately observed that integrating the mixture density over the control region leads to the identification of the signal strength as a ratio between the probability of observing an event in the control region under the mixture and background distributions.

$$\lambda(F, B) = 1 - \frac{F(\mathbb{C})}{B(\mathbb{C})} \quad (6)$$

Replacing  $F$  by its empirical estimate  $F_n$  leads to the plug-in estimator that compares the observed counts on the signal region to the expected background. This estimator is usually referred to as a counting experiment in the Physics literature [Behnke et al., 2013], and it is the semi-parametric efficient estimator of  $\lambda$ .

**Lemma 1.** *Under the model eq. (4) with known background, the plug-in estimator is*

$$\lambda(F_n, B) = 1 - \frac{F_n(\mathbb{C})}{B(\mathbb{C})} \quad (7)$$

*is the semiparametric efficient estimator. A level  $\alpha$  test based on this estimator is*

$$\Psi_\alpha(F_n, B) = I(T(F_n, B) > Z_{1-\alpha}) \quad (8)$$

$$\text{where } T(F_n, B) = \sqrt{n} \cdot \frac{F_n(\mathbb{S}) - B(\mathbb{S})}{\sqrt{F_n(\mathbb{S})(1 - F_n(\mathbb{S}))}} \quad (9)$$

*and  $Z_{1-\alpha}$  is the  $1 - \alpha$  quantile of the standard normal distribution.*

The proof can be found in Appendix B.2. We remark that physicists do not usually know the exact boundaries of the signal region, but they expect this contamination to be small. Consider the case where a  $\epsilon$  fraction of the signal leaks into the control region  $\int_{\mathbb{S}} s = 1 - \epsilon$ . Furthermore, assume that the amount of contamination  $\epsilon$  is smaller than  $B(\mathbb{C})$ . Then, we have that  $\lambda(F_n)$  underestimates the signal strength

$$E[\lambda(F_n)] = \lambda \cdot \left[ 1 - \frac{\epsilon}{B(\mathbb{C})} \right] \quad (10)$$

Consequently, the test eq. (8) is conservative whenever the signal leaks into the control region.

Usually, researchers do not know the background distribution. One might be tempted to replace  $T(F_n, B)$  for the estimate  $T(F_n, \hat{B})$  in the test eq. (8). However, the error term introduced by such replacement is not asymptotically negligible; see Appendix B.3. Fundamentally, this is due to the fact that the efficient estimator is robust to infinitesimal perturbations of the signal in the signal region rather than perturbations of the background. A natural next step is to consider the case where the background is parametric in eq. (4). That is,  $b = b_\gamma$  s.t.  $\gamma \in \mathbb{R}^K$ . To avoid the data on the signal region severely affecting the estimation of the background, a natural idea is to fit the background using only observations in the control region. This intuition leads to the maximum likelihood estimator that censors the signal region

$$(\gamma_*(F_n), \lambda_*(F_n)) = \arg \max_{\tilde{\gamma}, \tilde{\lambda}} \sum_{i=1}^n \ell(M_i, \tilde{\lambda}, \tilde{\gamma}) \quad \text{s.t.} \quad B_\gamma(\Omega) = 1 \quad (11)$$

$$\text{where } \ell(m, \lambda, \gamma) = I(m \in \mathbb{S}) \cdot \log((1 - \lambda) \cdot B_\gamma(\mathbb{S}) + \lambda) \quad (12)$$

$$+ I(m \in \mathbb{C}) \cdot \log((1 - \lambda) \cdot b_\gamma(m)). \quad (13)$$

The following lemma shows that this estimator is efficient when using a parametric background

**Lemma 2.** *Under the model eq. (4) with a parametric background, the censored MLE estimator eq. (11) is efficient and induces an asymptotic  $1 - \alpha$  level test.*

$$\Psi_\alpha^{(K)}(F_n) = I(\sqrt{n} \cdot \frac{\lambda_*(F_n)}{\tau_\lambda(F_n)}) > Z_{1-\alpha}. \quad (14)$$

The proof and the definition of  $\tau_\lambda(F_n)$  are deferred to Appendix B.4. Although the censored MLE does not provide a closed-form solution for  $\gamma_*(F_n)$ , looking at the first order optimality condition for the signal strength reveals that the efficient estimator is analogous to eq. (7) but using the estimated parametric background

$$\lambda_*(F_n) = 1 - \frac{F_n(\mathbb{C})}{B_{\gamma_*(F_n)}(\mathbb{C})} \quad (15)$$

Analogously to the test with known background eq. (8), if an  $\epsilon$  amount of signal leaks into the control region, the test eq. (14) loses power but retains validity. However, since the background is estimated from the data, there is a trade-off with respect to the size of the signal region. A small signal region implies substantial contamination of the control region, leading to poor background estimators and, consequently, low-power tests. Conversely, a rather large signal region leads to background estimators that cannot capture the background shape correctly, leading again to low-power tests. Finally, it is worth noting the censored MLE is equivalent to maximizing the conditional likelihood over the control region and extending it into the signal region, see Appendix B.7.

We remark that if the parametric form is taken to be a truncated series

$$b = b_\gamma = \sum_{k=1}^K \gamma_k \cdot \phi_k(x) \quad \text{where } \gamma \in \mathbb{R}^k, \quad (16)$$

an expectation-maximization algorithm Dempster et al. [1977] can be used to easily estimate the background parameters, see Appendix B.5. The resulting algorithm can be seen as a normalized version of the well-known D'Agostini iteration [Shepp and Vardi, 1982, D'Agostini, 1995] used in the unfolding problem Adye [2011].



In the experimental section, we use the  $K$ -th order Bernstein basis

$$\phi_k(x) = \binom{K}{k} \cdot x^k \cdot (1-x)^{K-k} \quad \text{and} \quad \frac{1}{K+1} \sum_{k=0}^K \gamma_k = 1 \quad (17)$$

where the restriction on  $\gamma$  guarantees that  $b_\gamma$  integrates to one. Polynomials in Bernstein form have been routinely used in the background modelling for high-energy physics [Rolandi, 2012, Harris et al., 2019] since they uniformly approximate any continuous function on  $\Omega$  at a rate of  $O(1/\sqrt{K})$  [Lorentz, 2013], and do not suffer from boundary bias [Ghosal, 2001]. Furthermore, in order to accelerate computations, we discretize the data before estimating the censored MLE, see Appendix B.6.

### 3 Simulation studies

In this section, we investigate the performance of our method for the detection of decaying high-pT W-boson events, Section 3.1, and high-mass resonance events, Section 3.2.

In all experiments, the data is split into training, validation, and test datasets. The training background and signal samples are used to fit a supervised probabilistic classifier. Let  $h : \mathcal{X} \rightarrow [0, 1]$  denote the trained classifier. Conditioned on the training dataset, the classifier is a deterministic function that predicts scores for each observation, with higher scores indicating that an event is more likely a signal event.

The validation dataset is used for three purposes. First, if performing decorrelation, the validation data is used to train the decorrelation algorithm by finding the optimal transport map on the validation background data and computing the transformed decorrelated classifier  $T_M(h)$ . Note that if decorrelation is not used, the transport map is defined as the identity map  $T_M(h) = h$ . Second, the validation dataset and the transformed classifier output are used to find the cut-off point that filters  $t\%$  of the background samples. To

do this, we compute the score  $T_M(h)$  of all background observations and find their  $t$ -th quantile, denoted by  $q(t)$ . Thus, the indicator function  $I(T_M(h(X)) \geq q(t))$  filters  $t\%$  of the background observations in the validation dataset.

Third, the validation dataset is used to calibrate the test. Namely, it is used to specify the signal region  $\mathbb{S}$  in eq. (4) and the degree  $K$  of the basis, see eq. (17). The signal region is fixed to be the interval between the 10% and the 90% quantiles of the empirical signal distribution in the validation dataset. That is, we allow for 20% of signal contamination in the control region. Inspecting the empirical distribution of the background, we find that the ratio between contamination and background in the control region, see eq. (10), ranges between 0.21-0.23 for the high-mass resonance experiments and 0.29-0.3 for the decaying high-pT W-boson experiments. Thus, on average, we expect to underestimate the true signal strength by 25%.

To fix the degree of the basis, we sub-sample  $N$  datasets of  $n$  background observations from the validation dataset. That is, these datasets follow the null distribution. Given a  $X_1, \dots, X_n \sim f$ , let  $\Psi_\alpha^{(K)}$  denote test eq. (14), where the parametric background eq. (16) is given by the Bernstein polynomial basis eq. (17). Then for  $K \in \{5, 10, 15, 20, 25, 30, 35, 40\}$ , we compute the empirical type I error and choose  $K$  such that the corresponding test is closest to the desired type I error. Concretely, we use the test  $\Psi_\alpha^{(K_*)}$  where

$$K_* = \arg \min_K \left| \alpha - \frac{1}{N} \cdot \sum_{j=1}^N \Psi_\alpha^{(K)}(F_n^{(j)}) \right| \quad (18)$$

and  $F_n^{(j)}$  is the empirical distribution of  $\{X_i^{(j)}\}_{i=1}^n$ . For all forthcoming experiments, we set  $\alpha = 0.05$ ,  $n = 20000$  and  $N = 500$ . Given the above test, a signal-enriched test can be built by first filtering observations using the trained classifier and then applying the test. Namely,

$$\Psi_\alpha^{(K_*)}(X, t) = \Psi_\alpha^{(K_*)}(\tilde{X}) \text{ where } X_i \in \tilde{X} \text{ if } I(C(X) \geq q(t)) \quad (19)$$

Thus, conditioned on the training and validation dataset  $\Psi_\alpha(\cdot, K_*, t)$  is a deterministic function.

Using the test dataset, we study the power of the signal-enriched test and the performance of the decorrelation algorithm (CDOT). To analyze the power of a signal detection test we proceed as follows: given a signal strength  $\lambda$ , we sub-sample  $N$  datasets of  $n$  observations from the test dataset, such that  $\lambda\%$  of those observations correspond to signal events. Then, for each dataset, we compute the empirical probability of rejecting the null hypothesis  $H_0 : \lambda = 0$ . Note that for  $\lambda = 0$ , that probability is the empirical type I error, while for  $\lambda \in \{0.01, 0.02, 0.05\}$  is the empirical type II error. In all cases, we report the empirical errors with their corresponding Clopper-Pearson confidence intervals. Finally, to understand the utility of the decorrelation algorithm, we study the power of the signal-enriched test when using a correlated and decorrelated classifier to filter observations.

### 3.1 Detection of decaying high-pT W-boson events

In the following, we consider the identification of decaying high-pT W-bosons, which is referred as W-tagging. W-tagging is one of the benchmark experiments used to compare decorrelation methods in particle physics. There is a detailed study of some existing decorrelation methods performed by the ATLAS collaboration [ATLAS, 2018b]. Hence, we use the W-tagging dataset used in Kasieczka and Shih [2020] and Kitouni et al. [2021] to compare our proposed decorrelation method to existing methods.

The SM background process in the dataset is considered to be events where gluons and light-flavor quarks hadronise into jets (represented by  $pp \rightarrow jj$ ), and the signal process is considered to be events with the SM production of two W-bosons (represented by  $pp \rightarrow WW$ ), with both W-bosons decaying into jets. The processes are simulated using Pythia

8.219 [Sjöstrand et al., 2008] with the condition that the initially produced particles have momentum,  $pT > 250$  GeV. The detectors are simulated using Delphes 3.4.1 [De Favereau et al., 2014], and the jets are reconstructed using FastJet 3.0.1 [Cacciari et al., 2012]. More details about the simulation can be found in Kasieczka and Shih [2020] and ATLAS [2018b]. The final selected dataset has jets that have mass  $m \in [50, 300]$  GeV and momentum  $pT \in [300, 400]$  GeV. The protected variable is the scaled invariant mass, whose range is  $\in [0, 1]$ . Table 1 in ATLAS [2018b] has a list of all the jet sub-structure variables related to the topology and structure of the jets that were used for training the auxiliary classifier. Additionally ‘label’ provides whether a particular event is signal (0) or background (1).

The data in Kasieczka and Shih [2020] is further split into training (background: 110k, signal: 250k), validation (background: 330k, signal: 80k) and test (background: 770k, signal: 80k) datasets. The training data is used to fit a supervised probabilistic random forest classifier with 1000 trees and minimal node size at 800 samples. The validation data is used to train the CDOT algorithm (1 using approach 1) with splits set at  $\{0.2, 0.4, 0.6\}$ , i.e., a different fixed optimal bandwidth is chosen for each of the intervals  $[0, 0.2]$ ,  $[0.2, 0.4]$ ,  $[0.4, 0.6]$ , and  $[0.6, 1]$  when training the kernel conditional distribution estimator.

Figure 4 shows the effect of sculpting on the background distribution when signal enrichment cuts are applied on the classifier output without any decorrelation. The plots show how the background distribution starts demonstrating a bump as the classifier output ( $h$ ) increases making it hard to detect the signal bump. Figure 5 shows the distributions of both the background and the signal after decorrelating the classifier using CDOT, i.e., the signal enrichment cuts are now applied on the decorrelated classifier output ( $T_M(h)$ ). As the decorrelated classifier output increases, the top row of the figure shows that the background distribution’s shape remains the same while the bottom row demonstrates the

increase in the signal proportion.

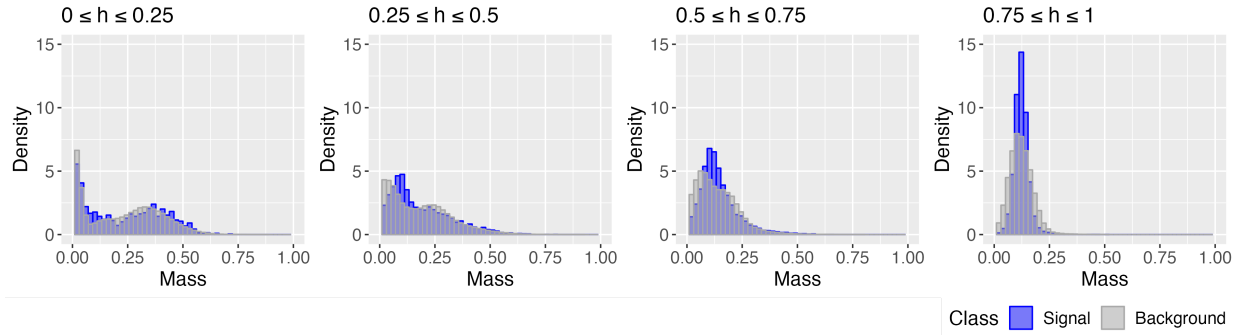


Figure 4: Density plots of the mass variable for the W-tagging data set after applying various thresholds on the classifier ( $h$ ) without any decorrelation. We observe sculpting (changes in shape) in the background.

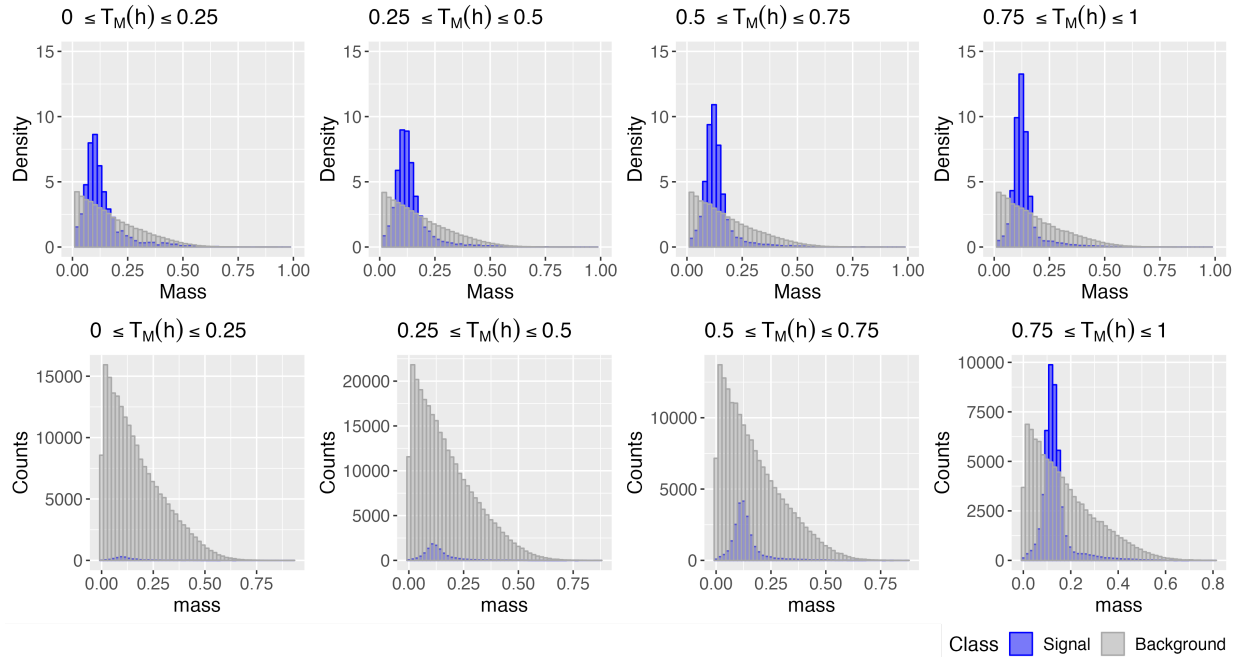


Figure 5: After decorrelation density plots (top row) and histograms (bottom row) of the mass variable for the W-tagging data set, applying various thresholds on the transformed classifier ( $T_M(h)$ ). We observe that cutting on the decorrelated classifier ( $T_M(h)$ ) instead of the classifier ( $h$ ) avoids sculpting.

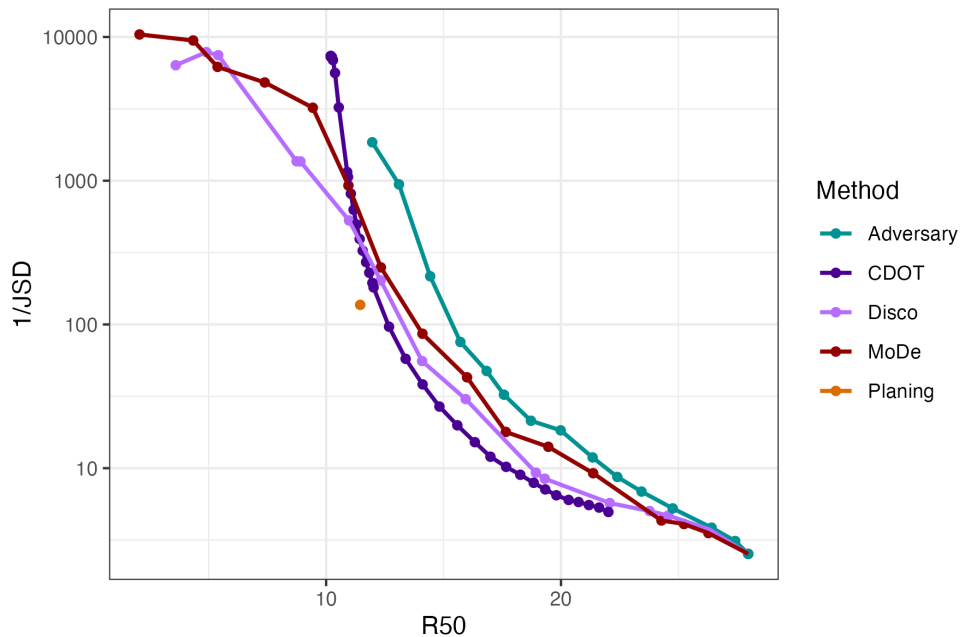


Figure 6: Decorrelation ( $1/\text{JSD}$  on  $\log_{10}$  scale) versus background-rejection power (R50) plot comparing CDOT to existing decorrelation methods.

Figure 6 compares the CDOT algorithm to existing state-of-the-art methods introduced in section 1.2 namely, Disco, Adversarial Neural Networks (ANN), MoDe, and Planing [El Naqa and Murphy, 2015]. We build on figure 7 presented in Kitouni et al. [2021] by adding the comparison of CDOT on the same comparison metrics as used in the figure. The plot compares the methods by looking at  $1/\text{JSD}$  versus R50, where R50 is the background rejection power (inverse false positive rate) at 50% signal efficiency and JSD is the Jensen Shannon divergence between the observations that are above the cut at 50% signal efficiency and the observations that are below the same cut. Higher R50 values represent good classifier performance in separating the signal from the background and higher  $1/\text{JSD}$  values represent higher decorrelation (independence) between the classifier and the protected variable for the background data. Figure 6 shows that while Disco is able to achieve higher decorrelation scores, at the expense of lower R50 values, looking at

around  $R_{50} = 10$  we see that CDOT is able to achieve higher decorrelation scores for a higher amount of accuracy. We also note that  $1/\text{JSD}$  as a metric is extremely sensitive as estimating JSD requires calculating the ratio of counts in pre-determined bins and the selection of the bins really influences the estimate. We choose the same binning that was used in Kitouni et al. [2021] but changing the binning even slightly changes the  $1/\text{JSD}$  scores.

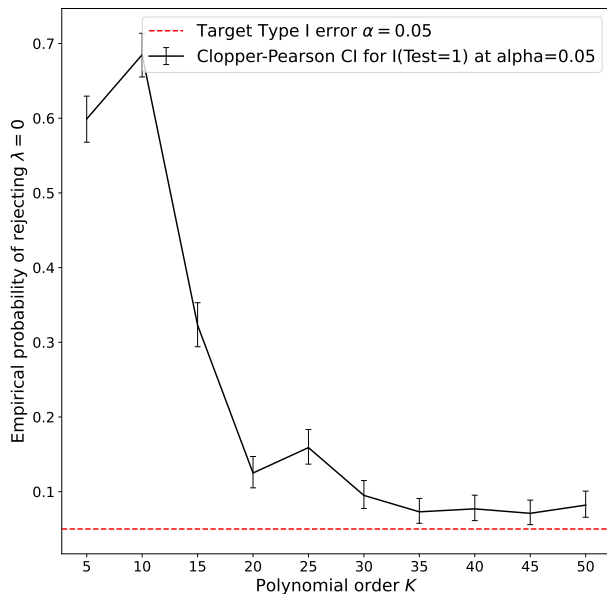


Figure 7: Model selection using simulated datasets composed only of background observations from the W-tagging validation dataset. The target type I error is 0.05. However, none of the asymptotic tests achieves it. The Bernstein basis of order 35 is selected, which achieves an average type I error between 0.05 and 0.1.

Regarding signal detection, Figure 7 displays the empirical probability of rejecting the null hypothesis under the null distribution. Based on it, we choose  $K_* = 35$  as the best-calibrated test. The corresponding p-value plots can be found in Appendix C.2. Using the test dataset, we perform a power analysis of the test as the correlated and decorrelated classifiers are used to filter more data; see Figure 8. Looking at Figure 9 and Figure 10, it is

clear that the decorrelated classifier does not produce sculpting under the null distribution, whereas the correlated classifier does. Consequently, the estimated background includes a bump in the signal region when using the correlated classifier. Hence, signal-enriched tests that use a correlated classifier become more conservative, as shown by the near-zero type I error, and lose power.

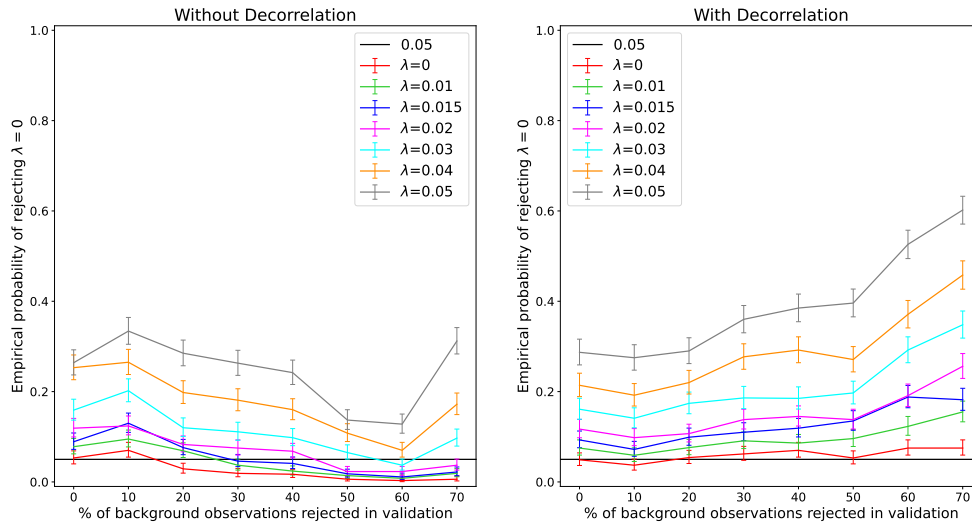


Figure 8: Power analysis using simulated datasets from the W-tagging test dataset. Clopper-Pearson intervals are shown for all estimates. The type I error ( $\lambda = 0$ ) and power ( $\lambda > 0$ ), when using the correlated and decorrelated classifiers is displayed.

Regarding the background estimation presented in Figures 9 and 10, we note that although all the information outside the signal region is used to estimate the background, the censored MLE test, see Figure 14, gives negligible weight to regions with low counts of events. Thus, the right tail of the invariant mass spectrum does not introduce bias in the background estimation.



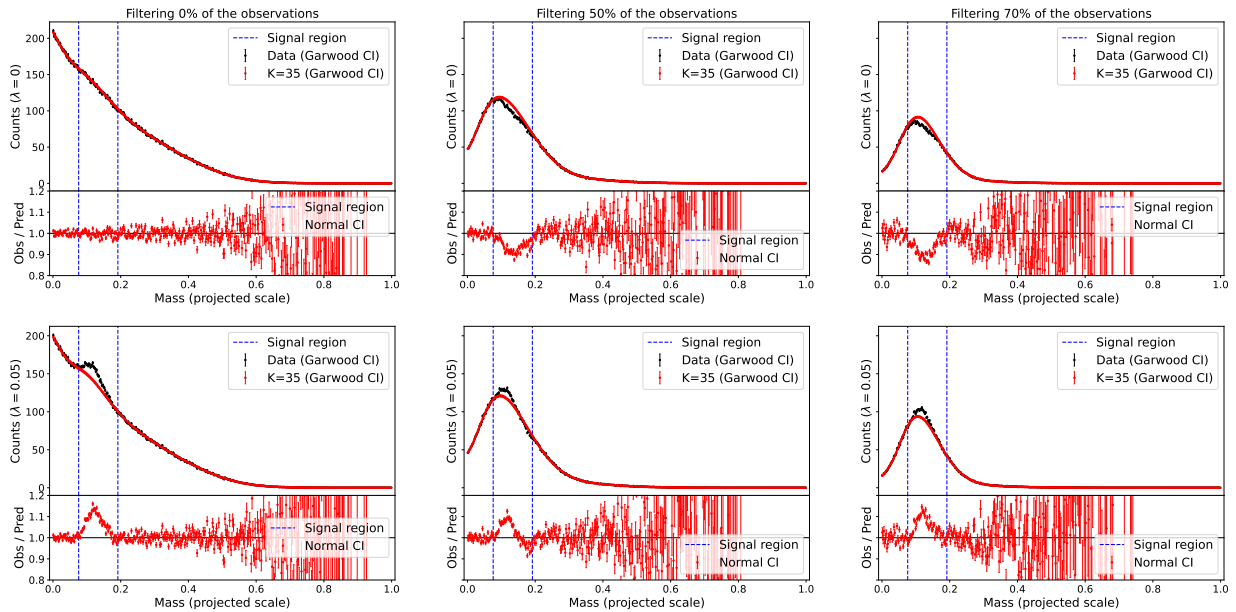


Figure 9: Background estimates for the W-tagging test dataset as more observations are filtered by a correlated classifier. The first row corresponds to the null hypothesis (no signal). In the second row, 5% of the data comes from the signal distribution. Note that the shape of the background distribution changes, producing a bump in the signal region.

### 3.2 Detection of high-mass resonance events

As mentioned in the introduction, high-mass resonance events are searched for where a high-mass particle is produced in proton proton collisions and decays into two Higgs bosons. Each of the two Higgs bosons subsequently decays hadronically into two b-quarks and hence to detect the signal one needs to investigate events where four b-quarks are observed. Additionally, in this case since the background simulations are not entirely reliable, we use this experiment to demonstrate the robustness of our entire pipeline to a misspecified background. For this purpose, we consider two kinds of background processes. The first dataset is a “4b” background dataset that includes QCD multijet events that produce four b-quarks. The second dataset is a “3b” background dataset which have four jets, of which

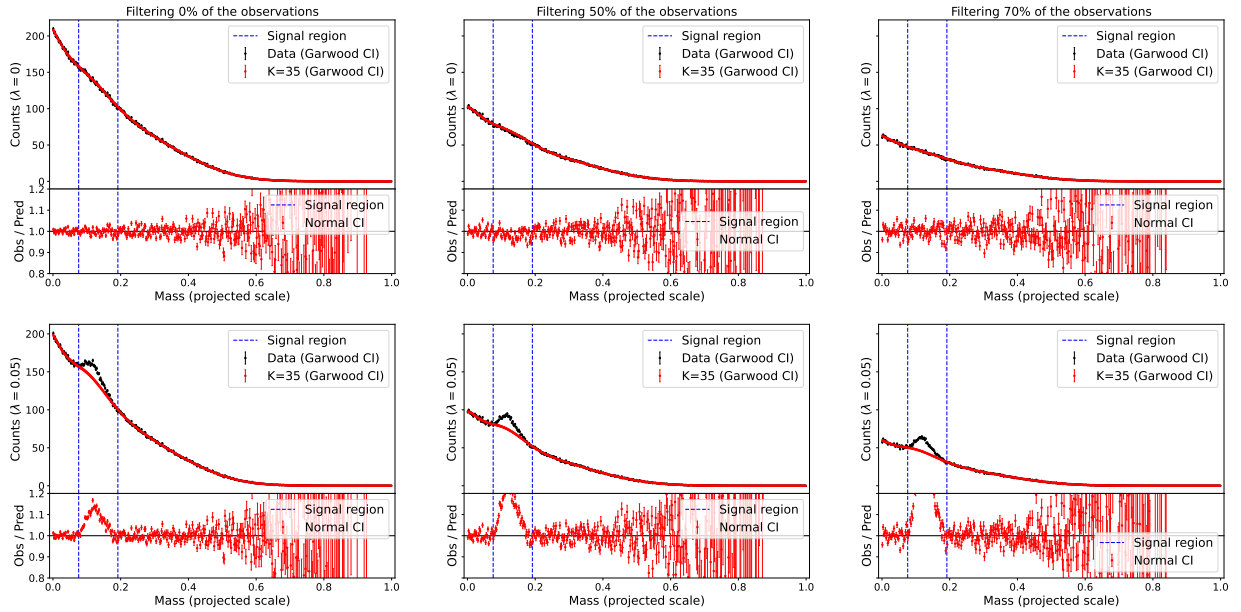


Figure 10: Background estimates for the W-tagging test dataset as more observations are filtered by the decorrelated classifier. The first row corresponds to the null hypothesis (no signal). In the second row, 5% of the data comes from the signal. Note that the shape of the background distribution does not change.

exactly three are b-jets. We generated the simulated collider data using the MadGraph particle physics software [Alwall et al., 2011]. We generated a high-mass resonance which result in four b-quarks (abbreviated  $X \rightarrow HH \rightarrow 4b$ ) with invariant mass of the resonance set at  $m \approx 400$  GeV.

We generated 463,848 3b events, 62,993 4b events, and 44,196 signal events. This was split into training data (3b: 50k, signal: 40k), validation data (3b: 120k) and test data (3b  $\approx$  294k, 4b  $\approx$  63k, signal  $\approx$  4k). The 3b and signal training data is used to fit a supervised probabilistic random forest classifier with 1000 trees and minimal node size set to 100 samples. The 3b validation data is used to train the CDOT algorithm 1 using approach 2. Finally, the performance of the decorrelation algorithm and the bump-hunting test are evaluated on the test data. To check the robustness of our procedure to

background misspecification, the classifier and CDOT training are only performed on the 3b background and not the 4b background, whereas the signal detection test is performed on the 4b background. Now, the kinematics of 3b events are similar, but not exactly the same, as those of 4b background events [CMS, 2022] and hence this is a good test of robustness of the pipeline.

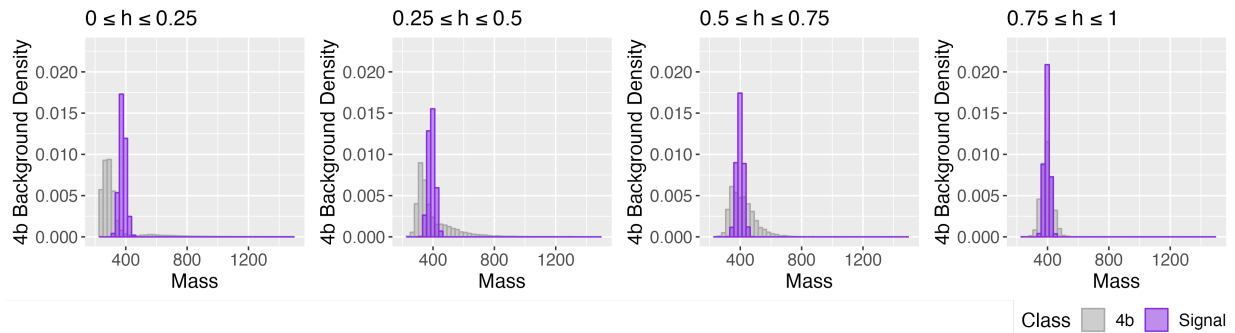


Figure 11: Density plots of the invariant mass for the 4b data set with signal after applying cuts on the classifier ( $h$ ) without any decorrelation. We observe sculpting.

Figure 11 shows the effect of sculpting produced on the 4b background when signal enrichment is performed using the correlated classifier. In contrast, Figure 12 displays the distributions after decorrelating the classifier using CDOT. Note that even though CDOT is trained on just the 3b background, it is robust to decorrelating both 3b test background as well as the 4b background.

Finally, we turn to signal detection. The proposed test, see eq. (14), depends on fitting the background with the Bernstein basis, see eq. (17), which is supported on the interval  $[0, 1]$ . Since the data sets 3b and 4b are not supported on the unit interval, we project them. A visual inspection of the 3b background data in the validation dataset indicates that it decreases exponentially. Thus, we transform all data in this section using the inverse CDF function of an exponential. Namely, given an observation, we apply the function

$m \rightarrow 1 - \exp \{-r \cdot (m - b)\}$  where  $b$  is the minimum invariant mass of the  $3b$  validation background and  $r = 0.003$ , which provide an adequate fit to the data.

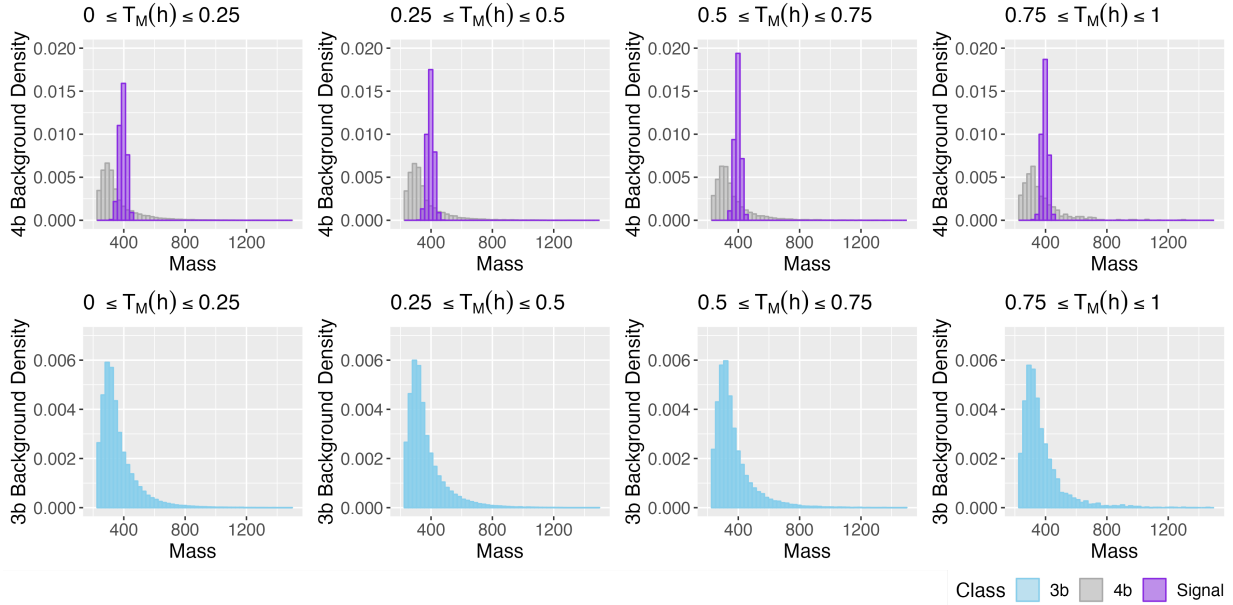


Figure 12: After decorrelation density plots of the invariant mass for the 4b data set with signal (top) and the test 3b background (bottom), applying cuts on the transformed classifier ( $T_M(h)$ ). We see that CDOT trained on 3b avoids sculpting 4b as well as 3b.

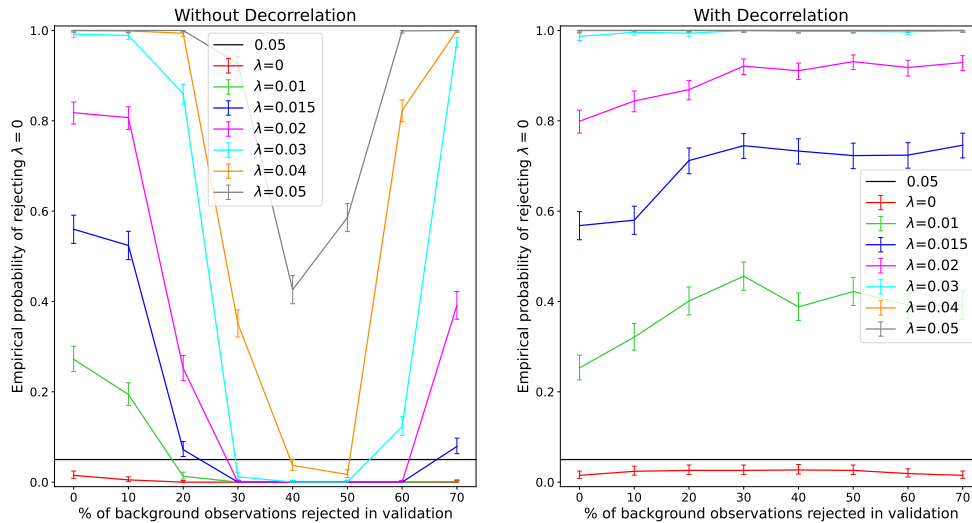


Figure 13: Validity and power analysis on the 3b test dataset.

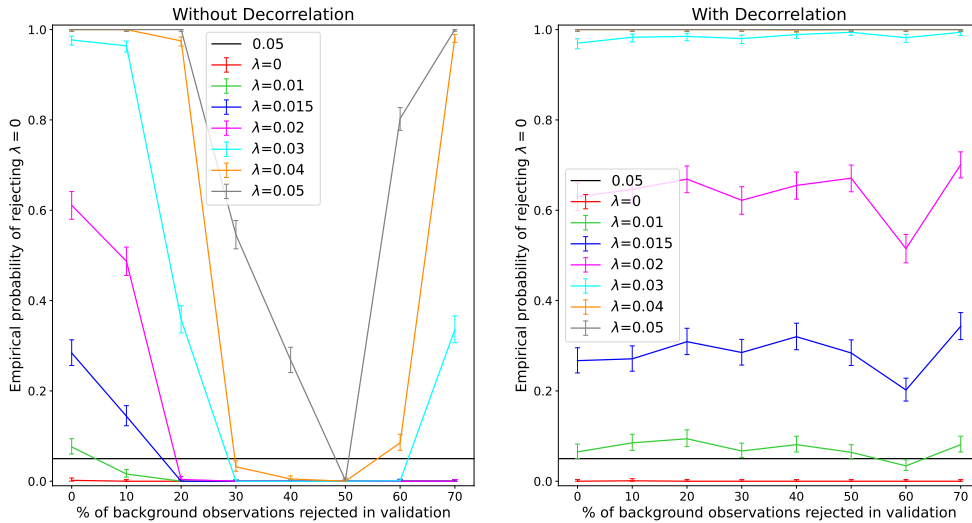


Figure 14: Validity and power analysis on 4b test dataset.

Analogously to the previous analysis, using the 3b validation dataset we find that  $K_* = 20$  provides the most calibrated test, the corresponding plots can be found in Appendix C.3. The power analysis with the 3b test dataset can be observed in Figure 13, while the 4b test dataset is displayed in Figure 14. When there is no distribution shift between the validation and test datasets, the intuition is the same as in the previous section. The decorrelated classifier preserves the shape of null distribution; hence, tests remain calibrated when enriched by a decorrelated classifier and increase their power. However, when there is a distribution shift between the validation and test datasets, we observe that the decorrelated classifier does not lead to an improvement in power, while the correlated classifier decreases the power. The plots displaying the background estimation have been deferred to Appendix C.3.

## 4 Discussion

In this paper, we implement the entire pipeline of signal detection in particle physics using bump hunting after performing signal enrichment using a decorrelated transformed classifier. We conclude from the experiments that both signal enrichment using cuts on a classifier as well as decorrelating the classifier before performing cuts, improves the power of the bump hunt signal detection test. We also demonstrate in Section 3.2 that the bump hunt test as well as the decorrelation algorithm proposed in this paper, CDOT, are robust to some background model misspecifications. In the future, it would be interesting to study the robustness of the procedures to different kinds of model mis-specifications.

We note that CDOT along with CNOTS [Algren et al., 2024] are post-processing decorrelation algorithms, meaning they can be applied to any pre-trained classifier to decorrelate them. The advantage of this is that we do not have to re-train the classifier again, lowering the computational cost of the whole procedure. It also has the advantage that domain experts can train a classifier for a particular application using their expert knowledge, and then use CDOT to decorrelate their pre-trained classifier. There may be some loss of signal detection power since we are optimizing the two problems, finding the optimal classifier and a decorrelated classifier, sequentially instead of together. From Section 3.1, it appears that CDOT competes with existing state-of-the-art decorrelation methods.

Finally, we note that although in this work we focused on univariate protected variables. The decorrelation algorithm can be directly applied to their multivariate protected variables. However, the proposed semi-parametric efficient test would have to be modified to use a multivariate score test as in Bickel et al. [2006].

**Acknowledgments** We thank Patrick Bryant, Ben Nachman, David Shih, Sara Algeri, Tudor Manole, Kenta Takatsu, and the participants of *Systematic Effects and Nuisance*

*Parameters in Particle Physics Data Analyses* workshop in Banff for useful discussions and comments on this work.

## References

Tim Adye. Unfolding algorithms and tests using RooUnfold, May 2011. [24](#)

Malte Algren, John Andrew Raine, and Tobias Golling. Decorrelation using optimal transport. *The European Physical Journal C*, 84(6):579, 2024. [10](#), [11](#), [12](#), [38](#)

Johan Alwall, Michel Herquet, Fabio Maltoni, Olivier Mattelaer, and Tim Stelzer. Madgraph 5: going beyond. *Journal of High Energy Physics*, 2011(6):1–40, 2011. [34](#)

ATLAS. Identification of hadronically-decaying w bosons and top quarks using high-level features as input to boosted decision trees and deep neural networks in atlas at  $\sqrt{s} = 13$  tev. Technical report, ATL-PHYS-PUB-2017-004, 2017a. [3](#)

ATLAS. Performance of top quark and w boson tagging in run 2 with atlas. Technical report, ATLAS-CONF-2017-064, 2017b. [3](#)

ATLAS. Observation of  $h \rightarrow bb$  decays and  $vh$  production with the atlas detector. *Physics Letters B*, 786:59–86, 2018a. [4](#)

ATLAS. Performance of mass-decorrelated jet substructure observables for hadronic two-body decay tagging in atlas. Technical report, ATL-PHYS-PUB-2018-014, 2018b. [3](#), [6](#), [8](#), [27](#), [28](#)

ATLAS Collaboration. Search for New Particles in Two-Jet Final States in 7 TeV Proton-Proton Collisions with the ATLAS Detector at the LHC. *Physical Review Letters*, 105

(16):161801, October 2010. ISSN 0031-9007, 1079-7114. doi: 10.1103/PhysRevLett.105.161801. [8](#)

Mark P Becker, Ilsoon Yang, and Kenneth Lange. Em algorithms without missing data. *Statistical Methods in Medical Research*, 6(1):38–54, 1997. doi: 10.1177/096228029700600104. PMID: 9185289. [55](#)

Olaf Behnke, Kevin Kröniger, Grégory Schott, and Thomas Schörner-Sadenius. *Data Analysis in High Energy Physics*. Wiley Online Library, 2013. [14](#), [22](#)

Peter J. Bickel, Ya’acov Ritov, and Thomas M. Stoker. Tailor-made tests for goodness of fit to semiparametric hypotheses. *The Annals of Statistics*, 34(2), April 2006. ISSN 0090-5364. doi: 10.1214/009053606000000137. [38](#)

Patrick Bryant. *Search for Pair Production of Higgs Bosons in the Four Bottom Quark Final State Using Proton-Proton Collisions at  $\sqrt{s} = 13$  Tev with the ATLAS Detector*. The University of Chicago, 2018. [4](#), [5](#)

Janice Button, George R. Kalbfleisch, Gerald R. Lynch, Bogdan C. Maglić, Arthur H. Rosenfeld, and M. Lynn Stevenson. Pion-pion interaction in the reaction  $\bar{p} + p \rightarrow 2\pi^+ + 2\pi^- + n\pi^0$ . *Physical Review*, 126(5):1858–1863, June 1962. doi: 10.1103/PhysRev.126.1858. [8](#)

Matteo Cacciari, Gavin P Salam, and Gregory Soyez. Fastjet user manual: (for version 3.0. 2). *The European Physical Journal C*, 72:1–54, 2012. [28](#)

CDF Collaboration. Global Search for New Physics with 2.0/fb at CDF. *Physical Review D*, 79(1):011101, January 2009. ISSN 1550-7998, 1550-2368. doi: 10.1103/PhysRevD.79.011101. [5](#), [7](#), [8](#), [13](#)



- Taoli Cheng, Jean-François Arguin, Julien Leissner-Martin, Jacinthe Pilette, and Tobias Golling. Variational autoencoders for anomalous jet tagging. *Physical Review D*, 107(1): 016002, 2023. [10](#)
- Georgios Choudalakis. On hypothesis testing, trials factor, hypertests and the BumpHunter, January 2011. [5](#), [8](#), [13](#)
- CMS. Observation of higgs boson decay to bottom quarks. *Physical review letters*, 121(12): 121801, 2018. [4](#)
- CMS. Search for higgs boson pair production in the four b quark final state in proton-proton collisions at  $\sqrt{s}=13$  tev. *arXiv preprint arXiv:2202.09617*, 2022. [35](#)
- Jack H. Collins, Kiel Howe, and Benjamin Nachman. Extending the Bump Hunt with Machine Learning. *Physical Review D*, 99(1):014038, January 2019. ISSN 2470-0010, 2470-0029. doi: 10.1103/PhysRevD.99.014038. [8](#)
- Glen Cowan, Kyle Cranmer, Eilam Gross, and Ofer Vitells. Asymptotic formulae for likelihood-based tests of new physics. *The European Physical Journal C*, 71(2):1554, February 2011. ISSN 1434-6044, 1434-6052. doi: 10.1140/epjc/s10052-011-1554-0. [8](#)
- Giulio D’Agostini. A multidimensional unfolding method based on bayes’ theorem. *Nuclear Instruments and Methods in Physics Research Section A: Accelerators, Spectrometers, Detectors and Associated Equipment*, 362(2-3):487–498, 1995. [24](#), [56](#)
- J De Favereau, Christophe Delaere, Pavel Demin, Andrea Giammanco, Vincent Lemaitre, Alexandre Mertens, and Michele Selvaggi. Delphes 3: a modular framework for fast simulation of a generic collider experiment. *Journal of High Energy Physics*, 2014(2): 1–26, 2014. [28](#)

- A. P. Dempster, N. M. Laird, and D. B. Rubin. Maximum Likelihood from Incomplete Data Via the EM Algorithm. *Journal of the Royal Statistical Society: Series B (Methodological)*, 39(1):1–22, 1977. ISSN 2517-6161. doi: 10.1111/j.2517-6161.1977.tb01600.x. [24](#), [53](#), [55](#)
- Biagio Di Micco, Maxime Gouzevitch, Javier Mazzitelli, and Caterina Vernieri. Higgs boson potential at colliders: Status and perspectives. *Reviews in Physics*, 5:100045, 2020. [4](#)
- James Dolen, Philip Harris, Simone Marzani, Salvatore Rappoccio, and Nhan Tran. Thinking outside the rocs: Designing decorrelated taggers (ddt) for jet substructure. *Journal of High Energy Physics*, 2016(5):1–19, 2016. [9](#)
- Issam El Naqa and Martin J Murphy. *What is machine learning?* Springer, 2015. [30](#)
- Lyndon Evans and Philip Bryant. LHC machine. *Journal of instrumentation*, 3(08):S08001, 2008. [2](#)
- Subhashis Ghosal. Convergence rates for density estimation with bernstein polynomials. *The Annals of Statistics*, 29(5):1264–1280, 2001. [25](#)
- Eilam Gross and Ofer Vitells. Trial factors for the look elsewhere effect in high energy physics. *The European Physical Journal C*, 70(1-2):525–530, November 2010. ISSN 1434-6044, 1434-6052. doi: 10.1140/epjc/s10052-010-1470-8. [8](#)
- Philip Coleman Harris, Dylan Sheldon Rankin, and Cristina Mantilla Suarez. An approach to constraining the higgs width at the lhc and hl-lhc. *arXiv preprint arXiv:1910.02082*, 2019. [25](#)
- Tristen Hayfield and Jeffrey S Racine. Nonparametric econometrics: The np package. *Journal of statistical software*, 27:1–32, 2008. [19](#), [48](#)

Gregor Kasieczka and David Shih. Disco fever: Robust networks through distance correlation. *arXiv preprint arXiv:2001.05310*, 2020. [10](#), [27](#), [28](#)

Gregor Kasieczka, Benjamin Nachman, David Shih, Oz Amram, Anders Andreassen, Kees Benkendorfer, Blaz Bortolato, Gustaaf Brooijmans, Florencia Canelli, Jack H. Collins, Biwei Dai, Felipe F. De Freitas, Barry M. Dillon, Ioan-Mihail Dinu, Zhongtian Dong, Julien Donini, Javier Duarte, D. A. Faroughy, Julia Gonski, Philip Harris, Alan Kahn, Jernej F. Kamenik, Charanjit K. Khosa, Patrick Komiske, Luc Le Pottier, Pablo Martín-Ramiro, Andrej Matevc, Eric Metodiev, Vinicius Mikuni, Inês Ochoa, Sang Eon Park, Maurizio Pierini, Dylan Rankin, Veronica Sanz, Nilai Sarda, Urous Seljak, Aleks Smolkovic, George Stein, Cristina Mantilla Suarez, Manuel Szewc, Jesse Thaler, Steven Tsan, Silviu-Marian Udrescu, Louis Vaslin, Jean-Roch Vlimant, Daniel Williams, and Mikaeel Yunus. The LHC Olympics 2020: A Community Challenge for Anomaly Detection in High Energy Physics. *Reports on Progress in Physics*, 84(12):124201, December 2021. ISSN 0034-4885, 1361-6633. doi: 10.1088/1361-6633/ac36b9. [8](#)

Ouail Kitouni, Benjamin Nachman, Constantin Weisser, and Mike Williams. Enhancing searches for resonances with machine learning and moment decomposition. *Journal of High Energy Physics*, 2021(4):1–23, 2021. [10](#), [27](#), [30](#), [31](#)

Samuel Klein and Tobias Golling. Decorrelation with conditional normalizing flows. *arXiv preprint arXiv:2211.02486*, 2022. [11](#)

Michael R. Kosorok. *Introduction to Empirical Processes and Semiparametric Inference*. Springer, New York, 2008. ISBN 978-0-387-74977-8 978-0-387-74978-5. [21](#)

S. Kullback and R. A. Leibler. On Information and Sufficiency. *The Annals of Mathematical Statistics*, 22(1):79–86, 1951. ISSN 0003-4851. [59](#)

- Qi Li and Jeffrey S Racine. Nonparametric estimation of conditional cdf and quantile functions with mixed categorical and continuous data. *Journal of Business & Economic Statistics*, 26(4):423–434, 2008. [19](#), [48](#)
- Qi Li, Juan Lin, and Jeffrey S Racine. Optimal bandwidth selection for nonparametric conditional distribution and quantile functions. *Journal of Business & Economic Statistics*, 31(1):57–65, 2013. [19](#), [48](#)
- George G Lorentz. *Bernstein polynomials*. American Mathematical Soc., 2013. [25](#)
- Gilles Louppe, Michael Kagan, and Kyle Cranmer. Learning to pivot with adversarial networks. *Advances in neural information processing systems*, 30, 2017. [3](#), [10](#)
- Louis Lyons. Open statistical issues in Particle Physics. *The Annals of Applied Statistics*, 2(3):887 – 915, 2008. doi: 10.1214/08-AOAS163. URL <https://doi.org/10.1214/08-AOAS163>. [2](#)
- Tudor Manole, Patrick Bryant, John Alison, Mikael Kuusela, and Larry Wasserman. Background modeling for double higgs boson production: Density ratios and optimal transport. *arXiv preprint arXiv:2208.02807*, 2022. [4](#)
- Eric A Moreno, Thong Q Nguyen, Jean-Roch Vlimant, Olmo Cerri, Harvey B Newman, Avikar Periwal, Maria Spiropulu, Javier M Duarte, and Maurizio Pierini. Interaction networks for the identification of boosted  $h \rightarrow b\bar{b}$  decays. *Physical Review D*, 102(1):012010, 2020. [11](#)
- Ian Moutl, Benjamin Nachman, and Duff Neill. Convolved substructure: analytically decorrelating jet substructure observables. *Journal of High Energy Physics*, 2018(5):1–26, 2018. [10](#)

Gigi Rolandi. Lhc results-highlights. *arXiv preprint arXiv:1211.3718*, 2012. 25

Lawrence A Shepp and Yehuda Vardi. Maximum likelihood reconstruction for emission tomography. *IEEE transactions on medical imaging*, 1(2):113–122, 1982. 24, 56

Chase Shimmin, Peter Sadowski, Pierre Baldi, Edison Weik, Daniel Whiteson, Edward Goul, and Andreas Søgaard. Decorrelated jet substructure tagging using adversarial neural networks. *Physical Review D*, 96(7):074034, 2017. 10

Torbjörn Sjöstrand, Stephen Mrenna, and Peter Skands. A brief introduction to pythia 8.1. *Computer Physics Communications*, 178(11):852–867, 2008. 28

A. W. van der Vaart. *Asymptotic Statistics*. Cambridge Series in Statistical and Probabilistic Mathematics. Cambridge University Press, Cambridge, UK ; New York, NY, USA, 1998. ISBN 978-0-521-49603-2. 13, 21, 48

Cédric Villani. *Topics in optimal transportation*, volume 58. American Mathematical Soc., 2021. 11, 21

## SUPPLEMENTARY MATERIAL

### A Derivation and implementation of CDOT

In this section, first we show that the transformed classifier we need in Section 2.1 is in fact given by the optimal transport map from the conditional density  $p_b(z|m)$  to  $p_b(z)$ , where  $Z = h(X)$ ,  $X \sim p_b$ , and  $M$  is the protected variable.

**Lemma 3.** *Given any two random variables  $(Z, M)$ , a map that minimizes  $\mathbb{E} [\|T_M(Z) - Z\|^2]$  subject to  $T_M(Z)$  independent of  $M$  and  $T_M(Z)$  has the same marginal distribution as  $Z$ , is given by the optimal transport map  $T_m$  from  $F_{z|m}$  to  $F_z$  under the  $\ell^2$  cost function, where  $F_{z|m}$  and  $F_z$  are the cdfs of  $Z|M$  and  $Z$  respectively.*

*Proof:* Let  $T_m$  denote the optimal transport map from  $F_{z|m}$  to  $F_z$ , then by definition  $T_m$  minimizes  $\mathbb{E} [c(Z, T_m(Z)) | M = m]$  for each  $m$  and  $P(T_m(Z) \leq t | M = m) = F_z(t)$ , where  $c(x, y)$  is the cost function. Now let  $f_m(Z)$  be any other map such that given  $M = m$ ,  $f_m(Z)$  is distributed as  $F_z$ , that is,  $P(f_m(Z) \leq t | M = m) = F_z(t)$ . Then, by definition, when the cost function is the  $\ell^2$  loss,  $c(x, y) = \|x - y\|^2$ ,

$$\mathbb{E} [\|T_m(Z) - Z\|^2 | M = m] dP(m) \leq \mathbb{E} [\|f_m(Z) - Z\|^2 | M = m] dP(m) \quad (20)$$

Then

$$\mathbb{E} [\|T_m(Z) - Z\|^2] = \int \mathbb{E} [\|T_m(Z) - Z\|^2 | M = m] dP(m) \quad (21)$$

$$\leq \int \mathbb{E} [\|f_m(Z) - Z\|^2 | M = m] dP(m) = \mathbb{E} [\|f_m(Z) - Z\|^2]. \quad (22)$$

This shows that  $T_m(Z)$  is independent of  $M$ , its marginal distribution is  $F_z$  and it minimizes  $\mathbb{E} [\|T_M(Z) - Z\|^2]$  among all such maps. Notice that in this result,  $M$  or  $Z$  can be of any dimension since the dimension does not enter in the argument.

In our case where we make the classifier output  $Z = h(X)$  independent of  $M$ , the form of the optimal transport map from  $F_{z|m}$  to  $F_z$  when  $h(X)$  and  $M$  are one-dimensional is derived by observing that by definition,

$$\begin{aligned} F_z(T_m(t)) &= P(T_m(Z) \leq T_m(t) | M = m) = F_{z|m}(t) \\ \implies T_m(t) &= F_z^{-1}(F_{z|m}(t)). \end{aligned}$$

The CDOT (Classifier Decorrelated via Optimal Transport) procedure is detailed below:

**Algorithm 1.** *CDOT decorrelated classifier output on the experimental data  $\mathcal{E}$ .*

*Input:*  $X_i \in \mathcal{B}$  (Training:  $\mathcal{B}_1$ , Validation:  $\mathcal{B}_2$ ),  $Y_j \in \mathcal{S}$ ,  $W_k \in \mathcal{E}$ ,  $M_{X_i}, M_{Y_j}, M_{W_k} \forall i, j, k$ .

*Output:*  $T_{M_k}(h(W_k))$ , decorrelated classifier output for every  $k$ .

1. *Train a probabilistic classifier  $h$  on  $X_i \in \mathcal{B}_1, Y_j \in \mathcal{S} \forall i, j$ , which gives the probability of being a signal event given the data.*
2. *Evaluate  $h(X_i), h(Y_j), h(W_k) \forall i, j, k$ .*
3. *Estimate the conditional distribution  $F_{z|m}$  for  $X_i \in \mathcal{B}_2$  ( $Z = h(X)$ ) using one of the two approaches.*
  - (a) *Approach 1: Choose splits in the range of  $M$  and estimate  $\widehat{F}_{z|m}$  in each split using a kernel conditional distribution estimator with fixed optimal bandwidths.*
  - (b) *Approach 2:*
    - i. *Estimate  $\widehat{\mu}(M_{X_i}) = \widehat{\mathbb{E}}[\text{logit}(h(X_i)) | \log(M_{X_i})]$  (non-parametric regression).*
    - ii. *Evaluate  $\widehat{\eta}_i = \text{logit}(h(X_i)) - \widehat{\mu}(M_{X_i})$ .*
    - iii. *Estimate  $\widehat{\sigma}^2(M_{X_i}) = \widehat{\mathbb{E}}[\widehat{\eta}_i^2 | \log(M_{X_i})]$  (non-parametric regression).*
    - iv. *Evaluate  $\widehat{\epsilon}_i = \widehat{\eta}_i / \widehat{\sigma}(M_{X_i})$ .*

v. Estimate  $\widehat{F}_{\epsilon|m}$  using a kernel conditional distribution estimator with a fixed optimal bandwidth on  $\epsilon_i$ 's given  $\log(M_{X_i})$ 's.

vi. Evaluate the conditional CDF on the experimental data using

$$\widehat{F}_{z|m}(h(W_k)) = \widehat{F}_{\epsilon|m}[(\text{logit}(h(W_k)) - \widehat{\mu}(M_{W_k})) / \widehat{\sigma}(M_{W_k})].$$

4. Estimate  $\widehat{F}_z(t)$  using the empirical marginal CDF estimator on the background data  $\mathcal{B}_2$ .

5. Evaluate the CDOT classifier output as  $T_{M_k}(h(W_k)) = \widehat{F}_z^{-1}(\widehat{F}_{z|m}(h(W_k)))$ .

Note that all the kernel conditional distribution (CCDF) estimators were obtained using the `npdist` function in the R package `np` [Li and Racine, 2008, Hayfield and Racine, 2008, Li et al., 2013]. The fixed optimal bandwidths in both approaches above were chosen using the least-squares cross validation method of Li and Racine [2008] and Li et al. [2013].

## B Signal detection in the density model

### B.1 CLT for Z-estimators

The following lemma is an informal version of the asymptotic normality theorem for Z-estimators presented in section 5.3 of van der Vaart [1998], we refer the reader to it for the specific regularity conditions needed. It should be noted that the result does not require probability measures to have a density. Hence, we use  $\int g dF$  to denote that we integrate the function  $g$  with respect to the measure  $F$ .

**Lemma 4.** *Let  $\theta(F)$  be the parameters that satisfies the following zero equation*

$$\int h(x, \theta(F)) dF(x) = 0. \tag{23}$$



Let  $F_n$  denote the empirical distribution. Then

$$\sqrt{n}(\theta(F_n) - \theta(F)) \xrightarrow{d} \mathcal{N}(0, \tau^2(F)) \quad (24)$$

$$\text{where } \tau^2(F) = \int \psi^2(F, x) dF(x) \quad (25)$$

$$\text{and } \psi(F, x) = - \left[ \int \frac{\partial h}{\partial \theta}(x, \theta(F)) dF(x) \right]^\dagger \cdot h(x, \theta(F)) \quad (26)$$

Consider a coordinate  $\lambda$  of  $\theta$ . Then

$$\sqrt{n} \left( \frac{\theta_\lambda(F_n) - \theta_\lambda(F)}{\sqrt{[\tau^2(F_n)]_{\lambda, \lambda}}} \right) \xrightarrow{d} \mathcal{N}(0, 1). \quad (27)$$

## B.2 Efficient estimator with known background

**Lemma 1.** Under the model eq. (4) with known background, the plug-in estimator is

$$\lambda(F_n, B) = 1 - \frac{F_n(\mathbb{C})}{B(\mathbb{C})} \quad (7)$$

is the semiparametric efficient estimator. A level  $\alpha$  test based on this estimator is

$$\Psi_\alpha(F_n, B) = I(T(F_n, B) > Z_{1-\alpha}) \quad (8)$$

$$\text{where } T(F_n, B) = \sqrt{n} \cdot \frac{F_n(\mathbb{S}) - B(\mathbb{S})}{\sqrt{F_n(\mathbb{S})(1 - F_n(\mathbb{S}))}} \quad (9)$$

and  $Z_{1-\alpha}$  is the  $1 - \alpha$  quantile of the standard normal distribution.

*Proof.* The score function for  $\lambda$  is  $g = (s - b)/f$ . Consider the parametric submodel

$f_t = (1 - \lambda)b + \lambda s(1 + t \cdot h)$  where  $h$  is supported on the signal region  $\mathbb{S}$  and it is mean zero

w.r.t. the signal. The nuisance tangent set is

$$\Lambda = \left\{ \frac{h \cdot s}{f} : \exists h \in \mathbb{H} \right\} \text{ where } \mathbb{H} = \left\{ h : \int h \cdot s = 0 \text{ and } \int_{\mathbb{S}} h = 1 \right\}. \quad (28)$$

The orthogonal projection of  $g$  onto  $\Lambda$  is given by

$$\Pi g = \inf_{h \in \mathbb{H}} \left\| g - \frac{hs}{f} \right\|_2^2 = \frac{f}{s} \left[ g - \frac{B(\mathbb{C})}{F(\mathbb{S})} \right] \cdot I_{\mathbb{S}}. \quad (29)$$

The efficient score  $g_*$  is  $g$  minus its projection onto  $\Lambda$ :

$$g_* = g - \Pi g = \frac{B(\mathbb{C})}{F(\mathbb{S})} \cdot I_{\mathbb{S}} - \frac{1}{1-\lambda} \cdot I_{\mathbb{C}}. \quad (30)$$

The efficient estimator is defined as the following z-estimator

$$\sum_{i=1}^n g_*(X_i, \hat{\lambda}) = 0 \implies \hat{\lambda} = 1 - \frac{F_n(\mathbb{S})}{B(\mathbb{C})}. \quad (31)$$

The efficient influence function is

$$\psi(F, x) = \left[ - \int \frac{\partial g_*}{\partial \lambda} f \right]^{-1} g_*(x) \quad (32)$$

$$= \frac{F(\mathbb{S})(1-\lambda)}{B(\mathbb{C})} \left[ \frac{B(\mathbb{C})}{F(\mathbb{S})} \cdot I(x \in \mathbb{S}) - \frac{I(x \in \mathbb{C})}{1-\lambda} \right] \quad (33)$$

$$= (1-\lambda) \cdot I(x \in \mathbb{S}) - \frac{F(\mathbb{S})}{B(\mathbb{C})} \cdot I(x \in \mathbb{C}) \quad (34)$$

and its variance is

$$\tau^2(F) = \int \psi^2(F, x) f(x) = (1-\lambda)^2 F(\mathbb{S}) + \frac{F^2(\mathbb{S})}{B(\mathbb{C})} (1-\lambda) \quad (35)$$

$$= (1-\lambda) \frac{F(\mathbb{S})}{B(\mathbb{C})}. \quad (36)$$

The asymptotic variance of  $\hat{\lambda}$  is  $\tau^2$ , verifying that it is efficient. We then have the following central limit theorem

$$\sqrt{n} \left( \frac{\lambda(F_n, B) - \lambda(F, B)}{\tau(F_n)} \right) \xrightarrow{d} \mathcal{N}(0, 1). \quad (37)$$

Under the null hypothesis,

$$\sqrt{n} \cdot \frac{\lambda(F_n, B)}{\tau(F_n)} \xrightarrow{d} \mathcal{N}(0, 1) \quad (38)$$

and consequently

$$\Psi_\alpha(F_n, B) = I(T(F_n, B) > Z_{1-\alpha}) \quad (39)$$

$$\text{where } T(F_n, B) = \sqrt{n} \cdot \frac{\lambda(F_n, B)}{\tau(F_n)} = \sqrt{n} \cdot \frac{F_n(\mathbb{S}) - B(\mathbb{S})}{\sqrt{F_n(\mathbb{S})(1 - F_n(\mathbb{S}))}} \quad (40)$$

is an asymptotic  $1 - \alpha$  level test. □

### B.3 Impossibility of replacing known background by plug-in estimator

The following lemma states that to replace the known background under the null hypothesis, we must have  $|\hat{B}(C) - B(C)| = o_p(n^{-1})$ . However, this is not achievable even when given an auxiliary sample from the background, unless excessively constraining assumptions are placed on the background.

**Lemma 5.** *Assume that the background mass in the control region is bounded away from zero*

$$\exists c > 0 \text{ s.t. } c < \min \{B(C), 1 - B(C)\} \quad (41)$$

and that  $\hat{B}$  is an estimator of the true background that does not depend on  $F_n$ . It follows that for  $\Psi_\alpha(F_n, \hat{B})$  to be an asymptotic  $1 - \alpha$  test, it must hold that  $|\hat{B}(C) - B(C)| = o_p(n^{-1})$

*Proof.* Recall that

$$\Psi_\alpha(F_n, B) = I(T(F_n, B) > Z_{1-\alpha}) \quad (42)$$

Let  $\hat{B}$  be an estimator of  $B$ , we have that  $T(F_n, \hat{B}) = T(F_n, B) + R$  where  $R = T(F_n, B) - T(F_n, \hat{B})$ . The first term converges to a standard normal. Hence, if the remainder converges faster to zero, i.e.,  $R = o_p(n^{-1/2})$ , under the null hypothesis, it follows that  $T(F_n, \hat{B})$  converges to a standard normal. Consequently,  $\Psi_\alpha(F_n, \hat{B})$  is an asymptotically valid test.

Note that

$$|R| = |T(F_n, B) - T(F_n, \hat{B})| = n^{1/2} \cdot \frac{|\hat{B}(S) - B(S)|}{\sqrt{F_n(S) \cdot (1 - F_n(S))}} \quad (43)$$

Under the null, it holds by the weak law of large numbers that

$$F_n(S) \xrightarrow{p} B(S) \quad (44)$$

Hence, since  $0 < B(C) < 1$ , it follows by the continuous mapping theorem that

$$\sqrt{\frac{F_n(S) \cdot (1 - F_n(S))}{B(S) \cdot (1 - B(S))}} \xrightarrow{p} 1 \quad (45)$$

Consequently,  $|T(F_n, B) - T(F_n, \hat{B})| = o_p(n^{-1/2})$  is implied by

$$|\hat{B}(C) - B(C)| = o_p\left(\frac{\sqrt{B(C) \cdot (1 - B(C))}}{n}\right) \quad (46)$$

Since  $B(C)$  is bounded away from zero and one, the condition is implied by  $|\hat{B}(C) - B(C)| = o_p(n^{-1})$ .  $\square$

## B.4 Efficient estimator with parametric background

**Lemma 2.** *Under the model eq. (4) with a parametric background, the censored MLE estimator eq. (11) is efficient and induces an asymptotic  $1 - \alpha$  level test.*

$$\Psi_\alpha^{(K)}(F_n) = I(\sqrt{n} \cdot \frac{\lambda_*(F_n)}{\tau_\lambda(F_n)}) > Z_{1-\alpha}. \quad (14)$$

*Proof.* The score function is  $g = (g_\lambda, g_\gamma)$  where

$$g_\lambda = (b_\gamma - s)/f \quad (47)$$

$$g_\gamma = \frac{1 - \lambda}{f} \cdot \frac{\partial b}{\partial \gamma} \quad (48)$$

Consider the sub-parametric model  $f_t = (1 - \lambda) \cdot b_\gamma + \lambda \cdot s \cdot (1 + t \cdot h)$  where  $h$  is supported on the signal region  $\mathbb{S}$  and it's mean zero w.r.t. the signal. That is, the nuisance tangent set is defined by

$$\Lambda = \left\{ \frac{h \cdot s}{f} : \exists h \in \mathbb{H} \right\} \text{ where } \mathbb{H} = \left\{ h : \int h \cdot s = 0 \text{ and } \int_{\mathbb{S}} h = 1 \right\} \quad (49)$$

The orthogonal projection of  $g$  onto  $\Lambda$  is given by

$$\Pi g = \inf_{h \in \mathbb{H}} \left\| g - \frac{hs}{f} \right\|_2^2 = \left[ g - \frac{E[g \cdot I_{\mathbb{S}}]}{F(\mathbb{S})} \right] I_{\mathbb{S}} \quad (50)$$

consequently, we obtain the efficient score by projecting to the orthogonal complement of  $\Lambda$

$$g^* = g - \Pi g = g \cdot I_{\mathbb{C}} + \frac{E[g \cdot I_{\mathbb{S}}]}{F(\mathbb{S})} I_{\mathbb{S}} \quad (51)$$

where

$$g_{\lambda}^* = \frac{B_{\gamma}(\mathbb{C})}{(1-\lambda)B_{\gamma}(\mathbb{S}) + \lambda} \cdot I_{\mathbb{S}} - \frac{1}{1-\lambda} \cdot I_{\mathbb{C}} \quad (52)$$

$$g_{\gamma}^* = \frac{1-\lambda}{(1-\lambda)B_{\gamma}(\mathbb{S}) + \lambda} \cdot \left( \int_{\mathbb{S}} \frac{\partial b_{\gamma}}{\partial \gamma} \right) \cdot I_{\mathbb{S}} + \frac{\partial b_{\gamma}}{\partial \gamma} \cdot \frac{1}{b_{\gamma}} \cdot I_{\mathbb{C}} \quad (53)$$

Then, the estimands of interest are

$$(\lambda_*(F), \gamma_*(F)) \text{ s.t. } \int g^*(x, \lambda_*(F), \gamma_*(F)) \cdot f(x) dx = 0 \quad (54)$$

that correspond to the following  $M$ -estimand

$$(\lambda_*(F), \gamma_*(F)) = \arg \max_{\tilde{\gamma}, \tilde{\lambda}} \int \ell(x, \tilde{\lambda}, \tilde{\gamma}) \cdot f(x) dx \text{ s.t. } B_{\gamma}(\Omega) = 1 \quad (55)$$

$$\text{where } \ell(x, \lambda, \gamma) = I(x \in \mathbb{S}) \cdot \log((1-\lambda)B_{\gamma}(\mathbb{S}) + \lambda) + I(x \in \mathbb{C}) \cdot \log((1-\lambda)b_{\gamma}(x)) \quad (56)$$

The efficient estimators are the corresponding plug-in estimators  $(\lambda_*(F_n), \gamma_*(F_n))$ . It is worth noting that the efficient estimator for the signal strength is the same as the efficient estimator with known background but replacing the known background for the estimated parametric background

$$\lambda_*(F_n) = 1 - \frac{F_n(\mathbb{C})}{B_{\gamma_*(F_n)}(\mathbb{C})} \quad (57)$$

However, there is no closed-form solution for the background parameters  $\gamma_*(F_n)$ . Thus, we propose a expectation-maximization Dempster et al. [1977] algorithm to solve for them in

[appendix B.5](#).

Regarding inference, by [lemma 4](#), it follows that the efficient influence function is

$$\psi(F, x) = \left[ \int \frac{\partial^2 \ell}{\partial \theta \partial \theta}(x, \theta_*(F)) \cdot f(x) dx \right]^{\dagger} \cdot \frac{\partial \ell}{\partial \theta}(x, \theta_*(F)) \text{ where } \theta_*(F) = (\lambda_*(F), \gamma_*(F)) \quad (58)$$

and its variance is  $\tau^2(F) = \int \psi(F, x) \cdot \psi^t(F, x) \cdot f(x) dx$  Furthermore, let  $\tau_\lambda(F_n) = \sqrt{\tau_{\lambda, \lambda}^2(F_n)}$ , it follows by [lemma 4](#) that

$$\sqrt{n} \left( \frac{\lambda_*(F_n) - \lambda}{\tau_\lambda(F_n)} \right) \xrightarrow{d} \mathcal{N}(0, 1) \quad (59)$$

Finally, under the null hypothesis, we have that  $\lambda = 0$ , and consequently the following is an asymptotic  $1 - \alpha$  level test

$$\Psi_\alpha(F_n) = I(T(F_n) > Z_{1-\alpha}) \quad (60)$$

$$\text{where } T(F_n) = \sqrt{n} \cdot \frac{\lambda_*(F_n)}{\tau_\lambda(F_n)} \quad (61)$$

□

## B.5 Expectation-Maximization for censored MLE

Henceforth, assume that the parametric background is given by a truncated series [eq. \(16\)](#), and recall the censored MLE estimator

$$(\gamma_*(F_n), \lambda_*(F_n)) = \arg \max_{\gamma, \lambda} \sum_{i=1}^n \ell(M_i, \lambda, \gamma) \text{ s.t. } B_\gamma(\Omega) = 1 \quad (62)$$

where the loss censors the signal region

$$\ell(m) = I(m \in \mathbb{S}) \cdot \log((1 - \lambda) \cdot (1 - B_\gamma(\mathbb{C})) + \lambda) + I(m \in \mathbb{C}) \cdot \log((1 - \lambda) \cdot b_\gamma(m)) \quad (63)$$

In the following let  $n_{\mathbb{S}}$  denote the number of observations in the signal region  $n_{\mathbb{S}} = \sum_{i=1}^n I(M_i \in \mathbb{S})$ , and  $n_{\mathbb{C}} = n - n_{\mathbb{S}}$  denote the number of observations in the control region.

The above optimization doesn't have a closed-form solution, but the first-order optimality conditions indicate that the solution satisfies the following equalities

$$\lambda_*(F_n) = 1 - \frac{F_n(\mathbb{C})}{B_{\gamma_*(F_n)}(\mathbb{C})}, \quad B_{\gamma_*(F_n)}(\Omega) = 1 \quad (64)$$

$$\text{and } \frac{B_{\gamma_*(F_n)}(\mathbb{C})}{F_n(\mathbb{C})} \cdot \phi_k(\mathbb{C}) = \frac{1}{n} \sum_{i=1}^n I(x \in \mathbb{C}) \cdot \frac{\phi_k(M_i)}{b_{\gamma_*(F_n)}(M_i)} \text{ for } 1 \leq k \leq K \quad (65)$$

In the following, we will see that we can use an Expectation-Maximization (EM) approximation [Dempster et al., 1977] to obtain an iterative algorithm that converges to solutions that satisfy the above equations. In particular, we will use the methodology push-forward by Becker et al. [1997], which approximates the origin loss function by an EM-like loss without using an statistical argument.

We start by introducing a guess for the solution of  $\gamma$  at the  $q$ th iteration

$$\max_{\gamma: B_\gamma(\Omega)=1} \sum_{i=1}^n \ell(M_i) = \max_{\lambda, \gamma: B_\gamma(\Omega)=1} n_{\mathbb{S}} \cdot \log((1-\lambda) \cdot (1 - B_\gamma(\mathbb{C})) + \lambda) + n_{\mathbb{C}} \cdot \log(1-\lambda) \quad (66)$$

$$+ \sum_{i=1}^n I(M_i \in \mathbb{C}) \cdot \log \left( \sum_{k=1}^K \gamma_k \cdot \phi_k(X_i) \cdot \frac{\gamma_k^{(q)} \cdot b_{\gamma^{(q)}}(M_i)}{\gamma_k^{(q)} \cdot b_{\gamma^{(q)}}(M_i)} \right) \quad (67)$$

Then, noting that  $b_{\gamma^{(q)}}(M_i) = \sum_{k=1}^K \gamma_k^{(q)} \cdot \phi_k(M_i)$ , we lower-bound the objective via Jensen's inequality

$$\max_{\lambda, \gamma: B_\gamma(\Omega)=1} n_{\mathbb{S}} \cdot \log((1-\lambda) \cdot (1 - B_\gamma(\mathbb{C})) + \lambda) + n_{\mathbb{C}} \cdot \log(1-\lambda) \quad (68)$$

$$+ \sum_{k=1}^K \sum_{i=1}^n I(M_i \in \mathbb{C}) \cdot \frac{\gamma_k^{(q)} \cdot \phi_k(M_i)}{b_{\gamma^{(q)}}(M_i)} \cdot \log \left( \frac{\gamma_k \cdot b_{\gamma^{(q)}}(M_i)}{\gamma_k^{(q)}} \right) \quad (69)$$

Finally, we remove the terms that are constant w.r.t. the optimization

$$\max_{\lambda, \gamma: B_\gamma(\Omega)=1} n_{\mathbb{S}} \cdot \log((1-\lambda) \cdot (1 - B_\gamma(\mathbb{C})) + \lambda) + n_{\mathbb{C}} \cdot \log(1-\lambda) \quad (70)$$

$$+ \sum_{k=1}^K a_k \cdot \gamma_k^{(q)} \cdot \log(\gamma_k) \quad (71)$$

where

$$a_k = \sum_{i=1}^n I(M_i \in \mathbb{C}) \cdot \frac{\phi_k(M_i)}{b_{\gamma^{(q)}}(M_i)} \quad (72)$$

Let  $(\lambda^{(q+1)}, \gamma^{(q+1)})$  denote the solution of the above system of equations. It follows that the solution must satisfy the following conditions

$$\lambda^{(q+1)} = 1 - \frac{F_n(\mathbb{C})}{B_{\gamma^{(q+1)}}(\mathbb{C})}, \quad B_{\gamma^{(q+1)}}(\Omega) = 1 \quad (73)$$

and

$$\text{for } 1 \leq k \leq K \quad \gamma_k^{(q+1)} = \gamma_k^{(q)} \cdot \frac{1 - B_{\gamma^{(q+1)}}(\mathbb{C}) + \frac{\lambda^{(q+1)}}{1-\lambda^{(q+1)}}}{n_{\mathbb{S}}} \cdot \frac{a_k}{\phi_k(\mathbb{C})} \quad (74)$$

$$= \gamma_k^{(q)} \cdot \frac{B_{\gamma^{(q+1)}}(\mathbb{C})}{F_n(\mathbb{C})} \cdot \frac{1}{\phi_k(\mathbb{C})} \cdot \frac{a_k}{n} \quad (75)$$

Solving the system of equations leads to a normalized D'Agostini iteration [Shepp and Vardi, 1982, D'Agostini, 1995] for  $\gamma^{(q+1)}$  that doesn't depend on  $\lambda^{(q+1)}$

$$\gamma_k^{(q+1)} = \frac{\tilde{\gamma}_k}{B_{\tilde{\gamma}}(\Omega)} \quad \text{where } \tilde{\gamma}_k = \gamma_k^{(q)} \cdot \frac{a_k}{\phi_k(\mathbb{C})} \quad (76)$$

Finally, note that at the fix point  $\gamma_{\infty}$ , eqs. (73) and (74) become eq. (64). Since eq. (62) is concave w.r.t.  $\gamma$ , the iteration converges to the unique maximizer. Ergo,  $\gamma^{(\infty)} = \gamma_*(F_n)$ , and consequently  $\lambda^{(\infty)} = \lambda_*(F_n)$ .

## B.6 Discretized censored MLE

An issue when implementing the efficient test in the continuous case eq. (60), is to obtain a stable and fast implementation of the influence function eq. (58), which requires the inversion of the empirical Hessian. In order to sidestep this issue, we discretize the data and rely on the discrete delta method to construct or asymptotically valid test. Henceforth, assume that the parametric background is given by a truncated series eq. (16) and discretize the density model eq. (4). That is, we partition the control region into  $L$  bins and take the whole signal region as one bin. Namely, define the disjoint sets

$$\mathbb{C} = \cup_{l=1}^L \mathbb{C}_l \quad \text{s.t. } \mathbb{C}_i \cap \mathbb{C}_j = \emptyset \quad \text{for } i \neq j \quad (77)$$

and their corresponding counts

$$n_{\mathbb{S}} = n \cdot F_n(\mathbb{S}) \quad \text{and } n_l = n \cdot F_n(\mathbb{C}_l) \quad \text{for } 1 \leq l \leq L \quad (78)$$



The counts follow a Multinomial distribution

$$(n_1, \dots, n_L, n_S) \sim \text{Multinomial}(n_C, p) \text{ where } p_l = (1 - \lambda)B_\gamma(\mathbb{C}_l) \text{ for } 1 \leq l \leq L \quad (79)$$

$$p_S = (1 - \lambda)B_\gamma(\mathbb{S}_l) + \lambda \quad (80)$$

Let  $\mathbb{F}_n(\mathbb{C})$  denote the estimated probabilities in the control region

$$\mathbb{F}_n(\mathbb{C}) = \left[ F_n(\mathbb{C}_1), \dots, F_n(\mathbb{C}_L) \right]^t \quad (81)$$

The discretized censored maximum likelihood estimator is

$$(\gamma_*(F_n), \lambda_*(F_n)) = \arg \max_{\gamma, \lambda} \ell(\mathbb{F}_n(\mathbb{C}), \lambda, \gamma) \text{ s.t. } B_\gamma(\Omega) = 1 \quad (82)$$

where

$$\ell(\mathbb{F}_n(\mathbb{C}), \lambda, \gamma) = (1 - F_n(\mathbb{C})) \cdot \log((1 - \lambda) \cdot (1 - B_\gamma(\mathbb{C})) + \lambda) \quad (83)$$

$$+ F_n(\mathbb{C}) \cdot \log(1 - \lambda) \quad (84)$$

$$+ \sum_{l=1}^L F_n(\mathbb{C}_l) \cdot \log(B_\gamma(\mathbb{C}_l)) \quad (85)$$

Following an analogous EM-approximation as in section [appendix B.5](#), we can derive the

following D'Agostini iteration that converges to  $\gamma_*(F_n)$

$$\gamma_k^{(q+1)} = \frac{\tilde{\gamma}_k}{B_{\tilde{\gamma}}(\Omega)} \text{ where } \tilde{\gamma}_k = \gamma_k^{(q)} \cdot \frac{a_k}{\phi_k(C)} \text{ and } a_k = \sum_{l=1}^L F_n(\mathbb{C}_l) \cdot \frac{\phi_k(\mathbb{C}_l)}{B_{\gamma^{(q)}}(\mathbb{C}_l)} \quad (86)$$

Note that the above iteration is the natural discretization of the continuous iteration

[eq. \(76\)](#). Finally,  $\lambda_*(F_n)$  can still be computed by the ration between observed to expected

$$\text{counts } \lambda_*(F_n) = 1 - \frac{F_n(\mathbb{C})}{B_{\gamma_*(F_n)}(\mathbb{C})}.$$

Noting that  $\lambda_*(F_n)$  is only a function of the counts in the control region, we can proceed analogously to [appendix B.5](#) and obtain a central limit by the discrete delta method. Let  $\mathbb{F}(\mathbb{C})$  denote the population vector of probabilities in the control region

$$\mathbb{F}(\mathbb{C}) = \left[ F(\mathbb{C}_1), \dots, F(\mathbb{C}_L) \right] \quad (87)$$

it follows by the central limit theorem that

$$\sqrt{n} \cdot (\mathbb{F}_n(\mathbb{C}) - \mathbb{F}(\mathbb{C})) \xrightarrow{d} \mathcal{N}(0, D) \quad (88)$$

where  $D \in \mathbb{R}^{(L-1) \times (L-1)}$ ,  $D_{l,l} = F(\mathbb{C}_l) \cdot (1 - F(\mathbb{C}_l))$  and  $D_{l,j} = -F(\mathbb{C}_l) \cdot F(\mathbb{C}_j)$  for  $j \neq l$ .

Thus, by the discrete delta method and Slutsky's theorem, we have that

$$\sqrt{n} \cdot \frac{\lambda_*(F_n) - \lambda_*(F)}{\sqrt{g(F_n)^t \cdot D_n \cdot g(F_n)}} \xrightarrow{d} \mathcal{N}(0, 1) \quad (89)$$

where  $g(F_n) = \nabla_{\mathbb{F}_n(\mathbb{C})} \lambda_*(F_n)$  is the gradient with respect to the empirical probabilities, and  $D_n$  is the empirical covariance matrix of the probabilities  $D_n \in \mathbb{R}^{(L-1) \times (L-1)}$ ,  $[D_n]_{l,l} = F_n(\mathbb{C}_l) \cdot (1 - F_n(\mathbb{C}_l))$  and  $[D_n]_{l,j} = -F_n(\mathbb{C}_l) \cdot F_n(\mathbb{C}_j)$  for  $j \neq l$ .

Finally, analogously to the efficient test in the continuous case [eq. \(60\)](#), we define our asymptotic  $1 - \alpha$  level test to be

$$\Psi_\alpha(F_n) = I(T(F_n) > Z_{1-\alpha}) \quad (90)$$

$$\text{where } T(F_n) = \sqrt{n} \cdot \frac{\lambda_*(F_n)}{\sqrt{g(F_n)^t \cdot D_n \cdot g(F_n)}} \quad (91)$$

## B.7 Equivalence between censored and conditional MLE

Consider the mixture model [eq. \(4\)](#) where the background is known to belong to the set  $\mathcal{B}$ . Since the signal vanishes in the control region, it follows that the conditional distribution of the mixture on the control region depends only on the background distribution

$$M|M \in C \sim \frac{f(m)}{F(\mathbb{C})} \cdot I(m \in \mathbb{C}) = \frac{b(m)}{B(\mathbb{C})} \cdot I(m \in \mathbb{C}) \quad (92)$$

A natural idea is to estimate the conditional background distribution on the control region, and then extend it to the signal region, that is, to force the estimated background to integrate to one on the whole domain. This is justified if there is a unique way of extending the conditional background, and consequently the conditional measure identifies the measure

on the whole domain. For instance, this is the case when the true background distribution is known to be a polynomial.

**Lemma 6 (Polynomial densities that agree on  $\mathbb{C}$  must agree on  $\Omega$ ).** *Let  $\mathcal{B}$  be some set of densities supported on  $\Omega$  such that  $b \in \mathcal{B}$  and for any  $\tilde{b} \in \mathcal{B}$  it holds that*

$$(0) \tilde{b} \text{ is a polynomial, } \tilde{b} \geq 0 \text{ and } \tilde{B}(\Omega) = 1 \quad (93)$$

Furthermore, consider the function  $d(f, g)$  in  $\mathcal{B} \times \mathcal{B}$  such that

$$(1) d(f, f) = 0 \quad (2) d(f, g) = 0 \implies f = g \text{ a.e.} \quad (3) d(f, g) \geq 0 \quad \forall f, g \in \mathcal{B} \quad (94)$$

then

$$b = \arg \min_{\tilde{b} \in \mathcal{B}} d( b, \tilde{b} ) = \arg \min_{\tilde{b} \in \mathcal{B}} d( \frac{b}{B(\mathbb{C})} \cdot I_{\mathbb{C}}, \frac{\tilde{b}}{\tilde{B}(\mathbb{C})} \cdot I_{\mathbb{C}} ) \quad (95)$$

The lemma allows us to rewrite the signal strength as a function of  $F$  by exploiting the equivalence in equation [eq. \(95\)](#). Namely,

$$\lambda^*(F) = 1 - \frac{F(\mathbb{C})}{B_F^*(\mathbb{C})} \text{ where } b_F^* = \arg \min_{\tilde{b} \in \mathcal{B}} d( \frac{f}{F(\mathbb{C})} \cdot I_{\mathbb{C}}, \frac{\tilde{b}}{\tilde{B}(\mathbb{C})} \cdot I_{\mathbb{C}} ) \quad (96)$$

Furthermore, consider using the Kullback-Leibler divergence [Kullback and Leibler, 1951] for  $d$ , then we obtain the conditional maximum likelihood estimator

$$\lambda^*(F_n) = 1 - \frac{F_n(\mathbb{C})}{B_{F_n}^*(\mathbb{C})} \quad (97)$$

where

$$b_{F_n}^* = \arg \max_{\tilde{b} \in \mathcal{B}} \sum_{i=1}^n I(M_i \in \mathbb{C}) \cdot \log \left( \frac{\tilde{b}(M_i)}{\tilde{B}(\mathbb{C})} \right) \text{ s.t. } \tilde{B}(\Omega) = 1 \quad (98)$$

Note that the condition  $\tilde{B}(\Omega) = 1$  guarantees the valid extension of the conditional density to the whole domain.

Finally, regardless of the uniqueness of the extended background, both the conditional and censored MLE coincide from an algorithmic point of view. Recall the censored maximum likelihood estimator is given by

$$(\lambda^*(F_n), b_{F_n}^*) = \arg \max_{\tilde{\lambda}, \tilde{b} \in \mathcal{B}: \tilde{B}(\Omega)=1} n_{\mathbb{S}} \cdot \left( (1 - \tilde{\lambda}) \cdot (1 - \tilde{B}(\mathbb{C})) + \tilde{\lambda} \right) \quad (99)$$

$$+ \sum_{i=1}^n I(M_i \in \mathbb{C}) \cdot \log \left( (1 - \tilde{\lambda}) \cdot \tilde{b}(M_i) \right) \quad (100)$$

The first order optimality condition for  $\lambda_*$  is given by [eq. \(97\)](#). Plugging the result back into the optimization [eq. \(99\)](#) gives us the conditional MLE objective [eq. \(98\)](#).

*Proof of [lemma 6](#).* Since  $b \in \mathcal{B}$ , by (1) and (3), it follows that the minimum must be achieved

$$d\left( \frac{b}{B(\mathbb{C})} \cdot I_{\mathbb{C}}, \frac{b^*}{B^*(\mathbb{C})} \cdot I_{\mathbb{C}} \right) = 0 \quad (101)$$

by (2), we know that the function must agree a.e. on the control region

$$\frac{b}{B(\mathbb{C})} = \frac{b^*}{B^*(\mathbb{C})} \text{ a.e. } x \in \mathbb{C} \quad (102)$$

by (0), we can extend the previous equation to all the domain

$$\frac{b}{B(\mathbb{C})} = \frac{b^*}{B^*(\mathbb{C})} \text{ a.e. } x \in \Omega \quad (103)$$

Integrating to both sides over  $\Omega$ , and using the fact that  $\tilde{B}(\Omega) = 1$  for all  $\tilde{b} \in \mathcal{B}$ , we get

$$B(\mathbb{C}) = B^*(\mathbb{C}) \quad (104)$$

and consequently  $b = b^*$  a.e.  $x \in \Omega$  □

## C Simulation details

### C.1 Code

The code to reproduce the experiments can be accessed at [https://github.com/lkania/signal\\_test](https://github.com/lkania/signal_test)

### C.2 W-tagging dataset

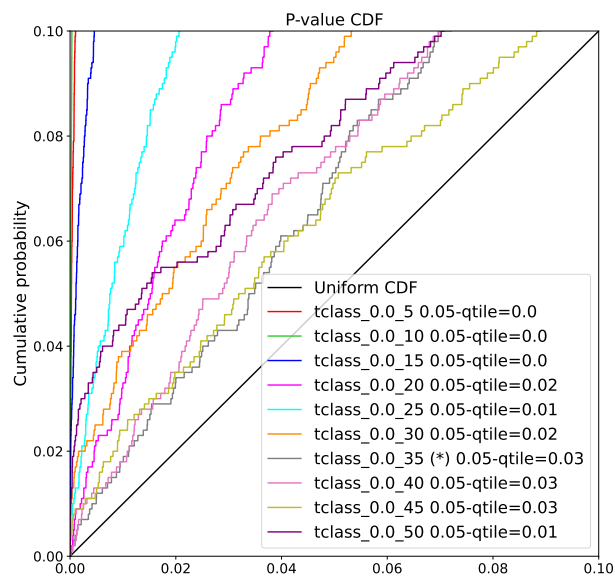


Figure 15: CDFs of the empirical pvalue distributions corresponding the different tests considered in figure 7.

### C.3 3b and 4b datasets

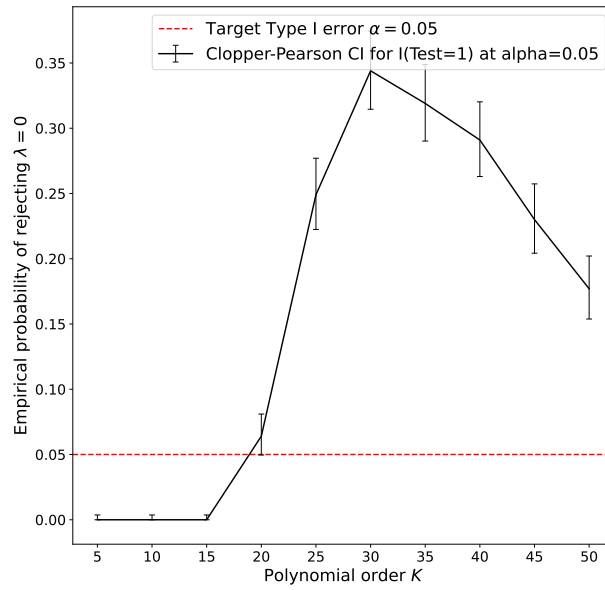


Figure 16: Model selection using simulated datasets composed only of background observations from the 3b validation dataset. The target type I error is 0.05. The Bernstein basis of order 20 is selected.

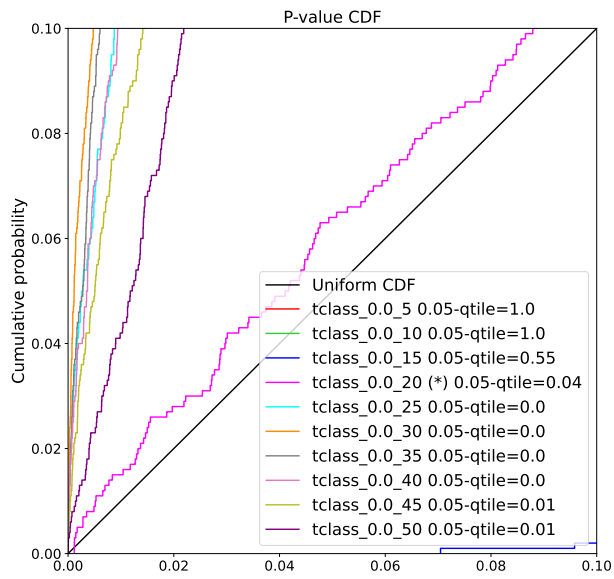


Figure 17: CDFs of the empirical pvalue distributions corresponding the different tests considered in figure 16.

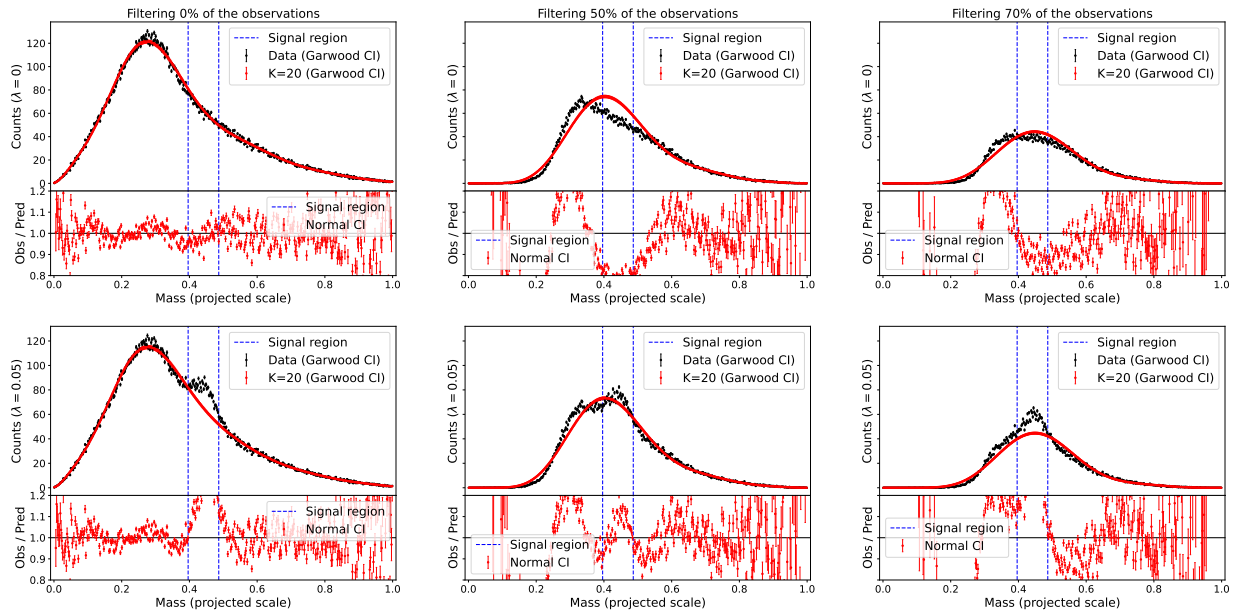


Figure 18: Background estimates for the 3b test dataset as the number of observations filtered by a correlated classifier is increased. The first row corresponds to the null hypothesis, i.e. no signal is present. In the second row, 5% of the data comes from the signal distribution. Note that the shape of the background distribution changes, producing a bump in the signal region.



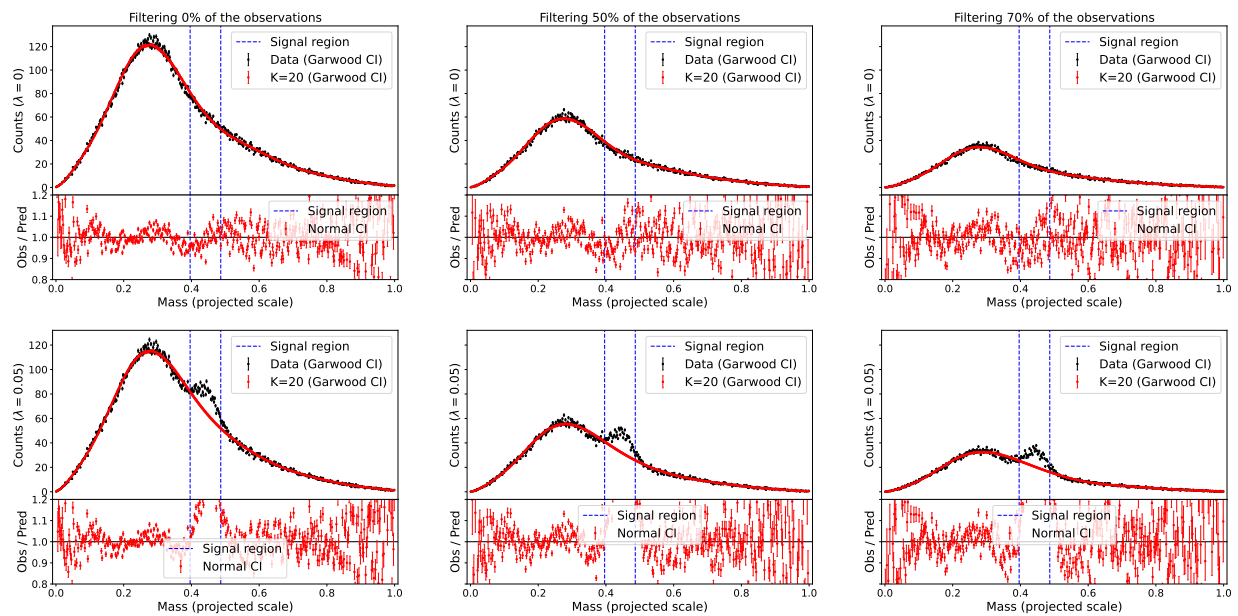


Figure 19: Background estimates for the 3b test dataset as the number of observations filtered by the decorrelated classifier is increased. The first row corresponds to the null hypothesis, i.e. no signal. In the second row, 5% of the data comes from the signal. Note that the shape of the background distribution does not change.

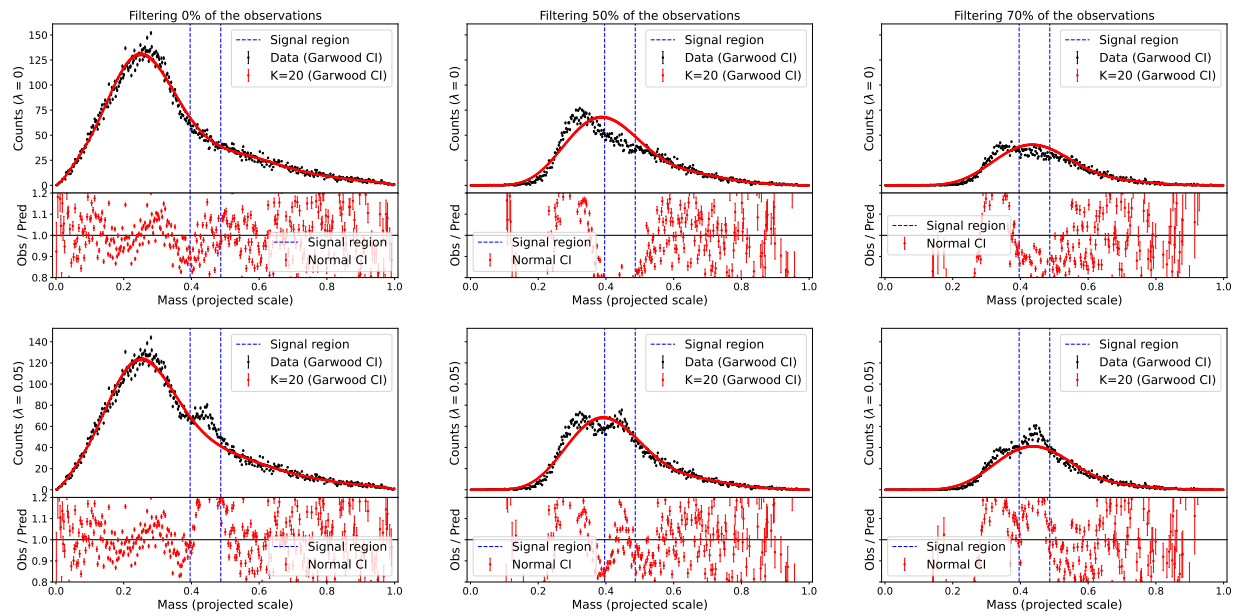


Figure 20: Background estimates for the 4b test dataset as the number of observations filtered by a correlated classifier is increased. The first row corresponds to the null hypothesis, i.e. no signal is present. In the second row, 5% of the data comes from the signal distribution. Note that the shape of the background distribution changes, producing a bump in the signal region.

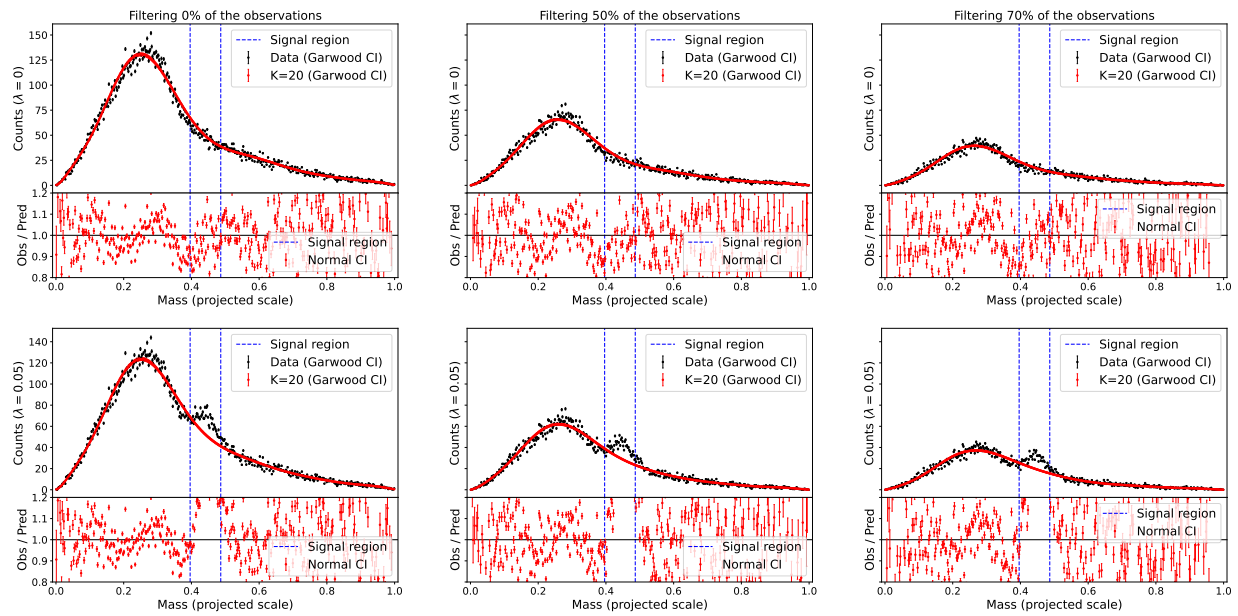


Figure 21: Background estimates for the 4b test dataset as the number of observations filtered by the decorrelated classifier is increased. The first row corresponds to the null hypothesis, i.e. no signal. In the second row, 5% of the data comes from the signal. Note that the shape of the background distribution does not change.